A&A 654, A77 (2021)
https://doi.org/10.1051/0004-6361/202141188

Astronomy & Astrophysics

Stellar Population Astrophysics (SPA) with TNG

Atmospheric parameters of members of 16 unstudied open clusters*

R. Zhang[1,2], S. Lucatello[2], A. Bragaglia[3], R. Carrera[2], L. Spina[2], J. Alonso-Santiago[4], G. Andreuzzi[5,6], G. Casali[7,8], E. Carretta[3], A. Frasca[4], X. Fu[8,3], L. Magrini[9], L. Origlia[3], V. D'Orazi[2], and A. Vallenari[2]

[1] Dipartimento di Fisica e Astronomia, Universita' di Padova, Vicolo Osservatorio 2, 35122 Padova, Italy
e-mail: ruyuan.zhang@studenti.unipd.it
[2] INAF-Osservatorio Astronomico di Padova, Vicolo Osservatorio 5, 35122 Padova, Italy
e-mail: sara.lucatello@inaf.it
[3] INAF-Osservatorio di Astrofisica e Scienza dello Spazio di Bologna, Via P. Gobetti 93/3, 40129 Bologna, Italy
[4] INAF-Osservatorio Astrofisico di Catania, Via S. Sofia 78, 95123 Catania, Italy
[5] Fundación Galileo Galilei – INAF, Rambla José Ana Fernández Pérez 7, 38712, Breña Baja Tenerife, Spain
[6] INAF-Osservatorio Astronomico di Roma, Via Frascati 33, 00078 Monte Porzio Catone, Italy
[7] Dipartimento di Fisica e Astronomia, Università degli Studi di Firenze, Via G. Sansone 1, 50019 Sesto Fiorentino, Firenze, Italy
[8] KIAA-The Kavli Institute for Astronomy and Astrophysics at Peking University, Beijing 100871, PR China
[9] INAF-Osservatorio Astrofisico di Arcetri, Largo E. Fermi, 5, 50125 Firenze, Italy

Received 27 April 2021 / Accepted 9 June 2021

ABSTRACT

Context. Thanks to the modern understanding of stellar evolution, we can accurately measure the ages of open clusters (OCs). Given their position, they are ideal tracers of the Galactic disc. *Gaia* data release 2, besides providing precise parallaxes, led to the detection of many new clusters, opening a new era for the study of the Galactic disc. However, detailed information on the chemical abundance for OCs is necessary to accurately date them and to efficiently use them to probe the evolution of the disc.
Aims. Mapping and exploring the Milky Way structure is the main aim of the Stellar Population Astrophysics project. Part of this work involves the use of OCs and the derivation of their precise and accurate chemical composition. Here, we aim to analyse a sample of OCs located within about 2 kpc from the Sun, with ages from about 50 Myr to a few gigayears.
Methods. We used HARPS-N at the Telescopio Nazionale *Galileo* and collected very high-resolution spectra (R = 115 000) of 40 red giant/red clump stars in 18 OCs (16 never or scarcely studied plus two comparison clusters). We measured their radial velocities and derived the stellar parameters ($T_{\rm eff}$, $\log g$, $v_{\rm micro}$, and [Fe/H]) based on equivalent width measurement combined with a 1D – LTE atmospherical model.
Results. We discuss the relationship between metallicity and Galactocentric distance, adding literature data to our results to enlarge the sample and also taking age into account. We compared the result of observational data with the findings of chemo-dynamical models. These models generally reproduce the metallicity gradient well. However, at young ages we find a large dispersion in metallicity, that is not reproduced by models. Several possible explanations are explored, including uncertainties in the derived metallicity. We confirm the difficulties in determining parameters for young stars (age < 200 Myr), which is attributable to a combination of intrinsic factors (activity, fast rotation, magnetic fields, etc) which atmospheric models cannot easily reproduce and which affect the uncertainty on parameters.

Key words. open clusters and associations: general – Galaxy: structure – Galaxy: disk – stars: abundances

1. Introduction

Most of our knowledge of stellar physics, of the ages of stars , and of their evolution has been acquired thanks to the study of star clusters, of their formation and evolution and of their stellar populations. This knowledge has very general bearing on our insight into a variety of astrophysical processes. Age dating stellar populations is necessary to investigate the formation of the Milky Way (e.g., Ness et al. 2016). The interpretation of light from simple stellar systems allows the building of population synthesis models used in studying the star formation history in other galaxies. The rate and timing of mass loss is a crucial ingredient in probing the chemical evolution and feedback processes in galaxies. For all this, stellar clusters are privileged probes and test cases.

Open clusters, in particular, provide key insights into the Galactic disc. These objects are made of coeval, chemically homogeneous, and dynamically bound groups of stars born from the same molecular cloud. With metallicities not too far from that of the Sun (−0.5 < [Fe/H] < 0.5, see e.g., Netopil et al. 2016; Donor et al. 2020; Casali et al. 2019), OCs are generally young (most of them are <1 Gyr, but there are clusters

* Based on observations made with the Italian Telescopio Nazionale *Galileo* (TNG) operated on the island of La Palma by the Fundación Galileo Galilei of the INAF (Istituto Nazionale di Astrofisica) at the Observatorio del Roque de los Muchachos. This study is part of the Large Program titled SPA - Stellar Population Astrophysics: the detailed, age-resolved chemistry of the Milky Way disc (PI: L. Origlia), granted observing time with HARPS-N and GIANO-B echelle spectrographs at the TNG.

with ages as high as 8–10 Gyr, see e.g., Kharchenko et al. 2013; Cantat-Gaudin et al. 2020) and range greatly in size: from loose associations with just a handful of stars to super star clusters, with as many as 10^4 members. As they form and evolve into (or in close proximity to) the Galactic disc, they are prone to stripping and disruption, and are in fact thought to be one of the main sources of field stars (e.g., Lada & Lada 2003).

Stellar populations in OCs cover stars from low to high mass, and different evolutionary stages, making each cluster a snapshot of stellar evolution at a given age and composition. With ages covering the entire lifespan of the thin disc, OCs trace the young, intermediate-age, and old thin disc components. Age can be measured for OCs with much more accuracy than for Galactic field stars, making them an ideal tool with which to probe Galaxy formation and evolution, through the age-metallicity relation, radial gradients and the comparison with theoretical models.

The *Gaia* results have brought a veritable revolution in our knowledge of OCs. High-probability memberships based on proper motions and parallaxes have been derived for very large samples of stars, leading also to the discovery of a substantial number of new OCs (see e.g., Cantat-Gaudin et al. 2018a; Castro-Ginard et al. 2019, 2020; Liu & Pang 2019; Sim et al. 2019).

Presently, only a small fraction of the known OCs have been studied with high-quality spectroscopic data, implying not only a lack of information on the composition for the vast majority of OCs, but also possibly inaccurate ages. A precise metallicity is a key ingredient for the derivation of ages from photometry (see e.g., Bossini et al. 2019). Moreover, the sample is likely to be affected by bias towards larger clusters, where, in the years before *Gaia* membership information, it was easier to successfully target actual members.

While *Gaia* will, at end of mission, provide distances and proper motions with a precision <10% for almost all known clusters, its spectroscopic capabilities are rather limited. The crucial third kinematic dimension (radial velocity, RV) and detailed chemical composition will need to be largely provided by ground-based complementary observations.

Recently completed and ongoing large stellar surveys, such as *Gaia*-ESO (GES), GALAH and APOGEE (Gilmore et al. 2012; De Silva et al. 2015; Majewski et al. 2017, respectively), provide composition and RVs for a few thousand stars in some hundreds of OCs based on high-resolution (~20–40 K) spectroscopy. This sample will be further increased by WEAVE (Dalton et al. 2020), one of the primary goals of which is the study of OCs as part of its Galactic Archeology Survey and likely by 4MOST (de Jong et al. 2019).

The key feature of GES and of the future surveys resides in their ability to study multiple members of the clusters in all evolutionary phases, with tens to many hundred of stars observed in each cluster (while e.g., APOGEE relies generally on much smaller samples). This is a crucial step in the understanding of the formation of the clusters (see e.g., Jeffries et al. 2014; Mapelli et al. 2015) and the evolution of the properties of the stars following changes in rotation, activity, and surface abundances, all key constraints to modern stellar evolutionary models (see e.g., Bertelli Motta et al. 2018; Smiljanic et al. 2016; Lagarde et al. 2019, on diffusion and extra mixing). However, because of their spectral coverage and/or resolution, these surveys provide an incomplete chemical characterisation of OC stars. An accurate determination of chemical abundances requires spectra of very high resolution and a wide spectral coverage, to measure the full set of the Fe-peak, CNO, α, p- and n-capture elements with high accuracy, on a par with the astrometric and photometric information provided by *Gaia*.

This implies that there is a need for observations that take a complementary approach, that is, that study a few stars per OC in detail with high-resolution (R > 50–70 000), large-wavelength-coverage, and high-signal-to-noise spectroscopy, deriving a full chemical characterization. Indeed, measuring elements of all nucleosynthetic chains, which probe different nuclear reaction sites in stars, means providing robust constraints to stellar evolutionary models and to the history of the Galactic disc.

This paper is part of a series presenting the findings of a large project called Stellar Populations Astrophysics (SPA), at the Italian TNG telescope. In this paper we will present the atmospheric parameters and radial velocities for stars in 16 OCs that have never been studied before or only poorly with high-resolution spectroscopy, plus two more as a comparison sample, while chemical abundance analysis will be presented in following papers.

In Sect. 2 we discuss the sample selection, followed by a description of observations and of the data-reduction procedure in Sect. 3. Determination of the spectroscopic parameters is discussed in Sect. 4, while in Sect. 5 we discuss our results in comparison with outcomes from the literature and chemo-dynamical models of the Galactic disc. Section 6 outlines our conclusions.

2. Target selection and dataset

In this work, we present the analysis of 40[1] giant stars in 18 open clusters, 16 of which have never been studied before, or only poorly, and two have been studied previously and are used as comparison samples. These clusters were selected because they are in the vicinity of the Sun, allowing us to obtain good-quality, high-resolution spectra, and are old enough to have stars evolved away from the main sequence. The target stars were not selected directly from the *Gaia* DR2 catalogue, but from the membership analysis done by Cantat-Gaudin et al. (2018a). We only targeted stars with high membership probability and we have from one (in 8 cases) to a maximum of seven stars (in 1 cluster) per OC.

We selected (almost) only red clump stars, not giants in general. Red clump stars are relatively homogeneous, and are bright enough (their absolute magnitude is $M_V \sim 0-1$ mag, Girardi 2016) to be observed at very high resolution in the Solar neighbourhood and at relatively large distance, and warm enough ($T_{\rm eff} \sim 4500-5700$ K, Girardi 2016) that they can be used to derive meaningful parameters and abundances. Their temperature is high enough to allow a precise abundance analysis, as opposed to cooler, upper red giant branch stars where line crowding (in particular at near solar metallicities) may hamper accurate analyses (see e.g., the discussion in Casali et al. 2020).

Table 1 shows information on the positions of OCs (both equatorial and Galactic coordinates) and some basic parameters, such as age, distance, reddening, and so on. All values come from a single homogeneous source, i.e., Cantat-Gaudin et al. (2020), where *Gaia* DR2 data are used to define candidate cluster members and derive cluster properties (see that paper for details).

All these OCs are located in the Galactic thin disc, cover the Galactocentric distance range 7.7–10 kpc, reside close to the Galactic midplane, and are in the age range from about 50 Myr to 4 Gyr. Figures 1 and 2 show the colour-magnitude diagrams (CMDs) in the *Gaia* system of the 18 OCs, based on the selection of Cantat-Gaudin et al. (2018a); the stars are coloured with

[1] We observed 41 stars, but one is a double-spectrum binary and was excluded from analysis.

Table 1. Properties of the observed clusters.

Cluster	RA (J2000)	Dec (J2000)	l (deg)	b (deg)	logAge (yr)	A_V (mag)	plx (mas)	pmRA (mas yr^{-1})	pmDE (mas yr^{-1})	Dist (pc)	R_{GC} (pc)	$\|z\|$ (pc)
ASCC 11	03:32:13.44	+44:51:21.6	150.546	−9.224	8.39	0.60	1.141	0.926	−3.030	867	9095	139
Alessi 1	00:53:22.32	+49:32:09.6	123.255	−13.33	9.16	0.08	1.390	6.536	−6.245	689	8726	159
Alessi-Teusch 11	20:16:30.48	+52:03:03.6	87.435	9.268	8.16	0.37	1.520	−0.139	−1.295	634	8335	102
Basel 11b	05:58:11.28	+21:57:54.0	187.442	−1.117	8.36	1.56	0.534	1.046	−4.137	1793	10121	34
COIN-*Gaia* 30	01:24:19.20	+70:34:26.4	125.684	7.878	8.41	1.25	1.346	−6.145	2.067	767	8804	105
Collinder 463	01:48:07.44	+71:44:16.8	127.391	9.358	8.06	0.79	1.137	−1.715	−0.307	849	8874	138
Gulliver 18	20:11:37.20	+26:31:55.2	65.527	−3.971	7.60	1.59	0.613	−3.198	−5.646	1595	7816	110
Gulliver 24	00:04:38.64	+62:50:06.0	117.62	0.447	8.25	1.05	0.636	−3.241	−1.57	1498	9131	11
Gulliver 37	19:28:18.48	+25:20:49.2	59.547	3.806	8.55	1.33	0.642	−0.775	−3.74	1438	7712	95
NGC 2437	07:41:46.80	−14:50:38.4	231.889	4.051	8.48	0.73	0.603	−3.838	0.365	1511	9345	106
NGC 2509	08:00:48.24	−19:03:21.6	237.844	5.840	9.18	0.23	0.363	−2.708	0.764	2495	9887	254
NGC 2548	08:13:38.88	−05:43:33.6	227.842	15.390	8.59	0.15	1.289	−1.313	1.029	772	8857	205
NGC 7082	21:28:44.64	+47:06:10.8	91.115	−2.859	7.79	0.79	0.729	−0.293	−1.106	1339	8472	66
NGC 7209	22:04:53.76	+46:30:28.8	95.480	−7.296	8.63	0.53	0.820	2.255	0.283	1154	8525	146
Tombaugh 5	03:47:56.16	+59:04:12.0	143.944	3.599	8.27	2.07	0.561	0.515	−2.388	1706	9768	107
UPK 219	23:27:24.96	+65:18:36.0	114.325	3.861	8.17	1.20	1.210	−1.734	−2.459	873	8735	58
				Comparison clusters								
Collinder 350	17:48:04.32	+01:31:30.0	26.952	14.773	8.77	0.52	2.708	4.965	−0.019	371	8021	94
NGC 2682	08:51:23.04	+11:48:50.4	215.691	31.921	9.63	0.07	1.135	10.986	−2.964	889	8964	470

Notes. All data come from Cantat-Gaudin et al. (2020) and are based on *Gaia* DR2.

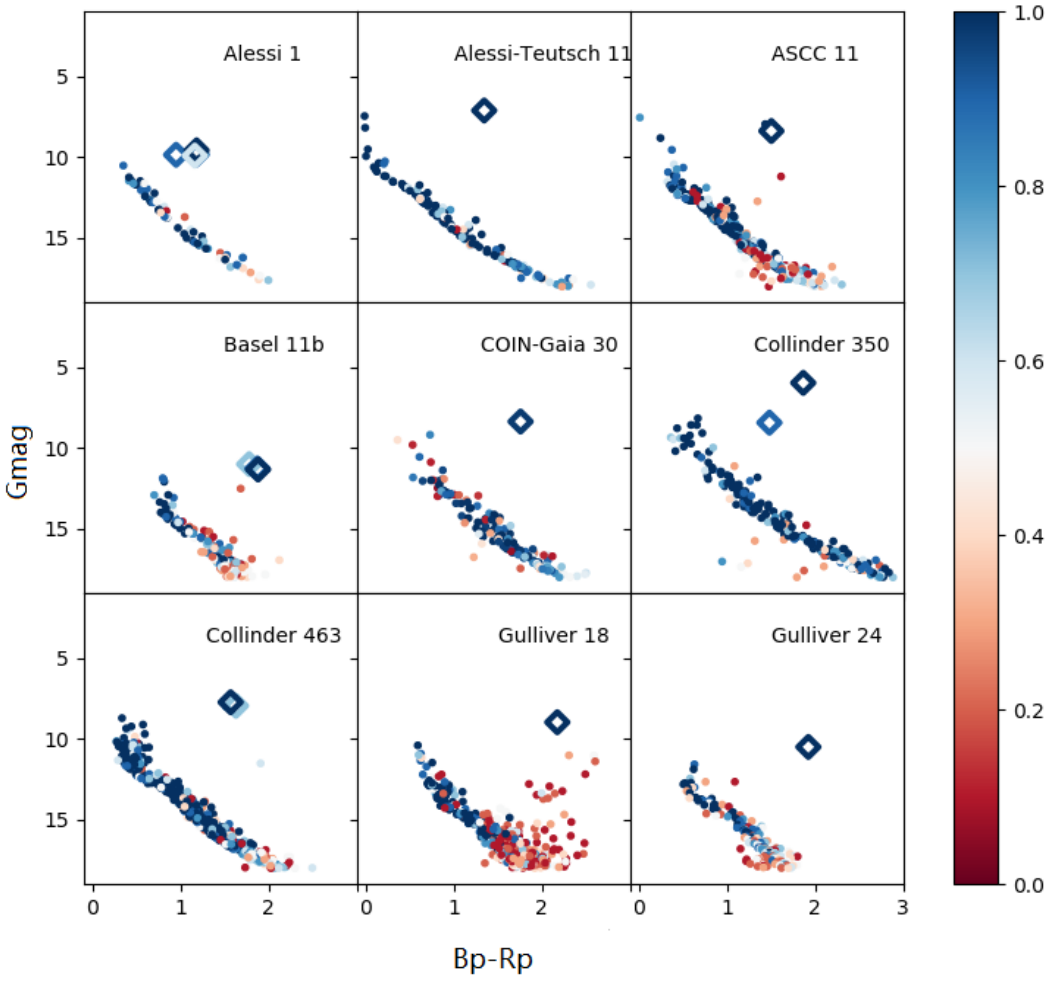

Fig. 1. Colour-magnitude diagrams of 9 the 18 open cluster. Dots are stars selected from the *Gaia* DR2 database, large diamonds show targets observed in this work. All points are coloured by membership probability (Cantat-Gaudin et al. 2018a).

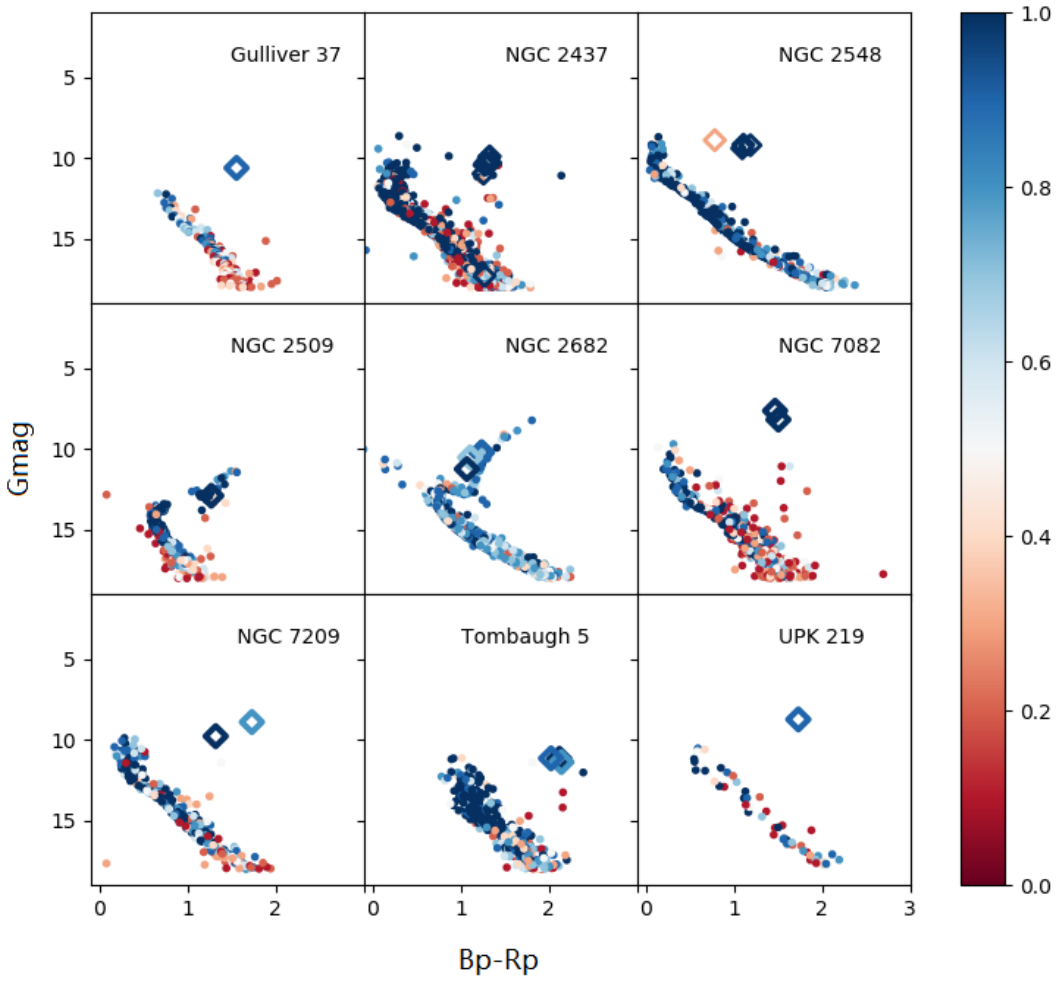

Fig. 2. As in Fig. 1 but for the remaining nine clusters.

membership probability and the observed targets are indicated by larger symbols.

3. Observation, data reduction and radial velocities

Observations were carried out in four observing runs in December 2018, and January, August, and December 2019. In most cases, multiple exposures were obtained (see Table A.1 for details on the individual targets). The exposure times varied according to the star magnitude and the sky conditions; the goal was to reach at least a signal-to-noise ratio (S/N) of 50 at 500 nm. We combined multi-exposure spectra before further data analysis.

All of those data were obtained with the 3.5 m Telescopio Nazionale *Galileo* (TNG) at El Roque de los Muchachos Observatory (La Palma, Canary Islands, Spain). We used the two high-resolution spectrographs HARPS-N and GIANO in GIARPS mode. This means that observation in the optical range and near-infrared (NIR) are executed at the same time with the light from a single target separated using a dichroic (a few more details can be found in previous SPA papers; see e.g., Frasca et al. 2019; D'Orazi et al. 2020). The analysis of GIANO data will be presented in forthcoming works; we deal here with the HARPS-N data. HARPS-N covers the wavelength range between 383 and 693 nm, with a resolution of $R = 115\,000$; this spectrograph is highly suitable for the determination of radial velocity (RV) and abundances with very high precision.

The spectra were reduced by the HARPS-N data reduction pipelines (they were corrected for bias and flat field, extracted to 1D spectra, wavelength calibrated and corrected for barycentric motion) and retrieved from the Italian Center for Astronomical Archives in Trieste[2]. Spectrum continuum normalisation with cubic splines and combination were done with IRAF[3] using the tasks CONTINUUM AND SCOMBINE.

The calculation of RV was done on the final normalised spectra with the IRAF task RVIDLINES, which measures the wavelength shift of a list of features. For all stars, the RV information and the errors are given in Table 2, together with the S/N measured at 600 nm. As we selected high-probability members, we find very similar RVs for stars belonging to the same cluster, which further reinforces their membership.

All but one of our stars (plus the binary) have an RV determined with the RVS instrument on board *Gaia*, which observes the NIR Ca II triplet region at a resolution of $R = 11\,500$. These RVs and the corresponding errors, from *Gaia* DR2, are also presented in Table 2.

Figure 3 shows the distribution of RV offsets between the value determined in this work and that from *Gaia*. These offsets

[2] http://archives.ia2.inaf.it/tng/

[3] IRAF is distributed by the National Optical Astronomy Observatory, which is operated by the Association of the Universities for Research in Astronomy, inc. (AURA) under cooperative agreement with the National Science Foundation.

Table 2. Radial velocities of targets.

Name	*Gaia* ID	S/N (600 nm)	RV km s^{-1}	σRV km s^{-1}	RV(*Gaia*) km s^{-1}	σRV(*Gaia*) km s^{-1}	Notes
ASCC 11	241730418805573760	93	−13.36	0.15	−13.87	0.23	
Alessi 1_1	402506369136008832	93	−5.50	0.05	−4.19	0.64	
Alessi 1_2	40250599117880752	88	−3.13	0.07	−5.23	0.81	
Alessi 1_3	402867593065772288	127	−4.57	0.20	−4.25	1.83	
Alessi 1_4	402880684126058880	120	−4.29	0.03	−4.54	0.42	
Alessi-Teusch 11	2184332753719499904	126	−27.11	0.12	−27.09	0.17	
Basel 11b_1	3424056131485038592	125	2.26	0.18	3.11	0.49	
Basel 11b_2	3424055921028900736	86	1.68	0.15	5.81	1.11	
Basel 11b_3	3424057540234289408	66	2.57	0.15	2.71	1.12	
COIN-*Gaia* 30	532533682228608384	93	−26.66	0.13	−26.10	0.14	
Collinder 463_1	534207555539397888	143	−9.68	0.16	−12.47	0.14	
Collinder 463_2	534363067715447680	152	−11.64	0.12	−11.62	0.14	
Gulliver 18	1836389309820904064	87	−1.97	0.18	−3.32	0.21	
Gulliver 24	430035249779499264	78	−30.37	0.16	−31.86	0.49	
Gulliver 37	2024469226291472000	78	−4.59	0.17	2.52	8.22	Binary? (see text)
NGC 2437_1	3029609393042459392	64	49.77	0.11	50.07	0.61	
NGC 2437_2	3029202711180744832	111	47.16	0.14	46.80	0.50	
NGC 2437_3	3030364134752459904	95	49.02	0.17	48.80	0.25	
NGC 2437_4	3029132686034894592	128	49.93	0.15			
NGC 2437_5	3029156222454419072	50	49.37	0.17	49.34	0.17	
NGC 2437_6	3029207006148017664	72	27.12	0.17	28.76	9.91	$P \sim 3350^d$ (Mermilliod et al. 2007)
NGC 2437_7	3029226694277998080	74	49.53	0.19	51.60	0.62	
NGC 2509	5714209934411718784	128	61.63	0.14	61.42	1.45	
NGC 2548_1	3064481400744808704	125	9.06	0.14	8.68	0.29	
NGC 2548_2	3064537647636773760	138	8.16	0.03	8.83	0.31	
NGC 2548_3	3064579703955646976	77	8.01	0.04	8.76	0.22	
NGC 2548_4	3064486692144030336	94	8.98	0.10	8.10	0.67	SB (Mermilliod et al. 2008)
NGC 7082_1	1972288740859811072	144	−11.89	0.15	−11.07	0.19	
NGC 7082_2	1972288637780285312	151					Double lined binary
NGC 7209_1	1975004019170020736	81	−19.00	0.16	−18.14	0.27	
NGC 7209_2	1975002919658397568	161	−17.98	0.15	−18.89	0.35	
Tombaugh 5_1	473266779976916480	72	−23.03	0.15	−22.05	1.03	
Tombaugh 5_2	473275782228263296	54	−22.63	0.12	−22.84	0.26	
Tombaugh 5_3	473268424940932864	53	−20.53	0.13	−23.45	0.29	
UPK 219	2209440823287736064	81	−0.07	0.15	−2.03	0.55	
Comparison clusters							
Collinder 350_1	4372743213795720704	240	−13.98	0.17	−14.57	0.20	
Collinder 350_2	4372572888274176768	70	−16.30	0.13	−14.73	0.16	
NGC 2682_1	604921512005266048	141	33.63	0.23	34.29	0.30	
NGC 2682_2	604920202039656064	78	34.93	0.14	34.49	0.35	
NGC 2682_3	604904950611554432	82	33.93	0.20	36.83	0.96	Binary (see Table 5)
NGC 2682_4	604917728138508160	53	27.41	0.13	26.98	2.70	Binary (see Table 5)

are generally small with an average offset of -0.11 ± 1.89 km s^{-1}. Owing to our small sample we made no further comparisons.

The few discrepant values seem likely to be due to the much larger errors in the *Gaia* RVS determinations or to binarity. Two stars in NGC 2682, namely numbers 3 and 4 in our list, one in NGC 2437, namely number 6 in our list, and one in NGC 2548, namely number 4 in our list, are known binaries (Mermilliod et al. 2007, 2008; Geller et al. 2021). The only Gulliver 37 star observed shows a large *Gaia* RV dispersion, 8.2 km s^{-1} based on 11 transits, with an average RV of 2.5 km s^{-1}, compared to our value of −4.59 km s^{-1}. Moreover, we have a high-resolution optical spectrum from another project from which we derived a RV of 21.92 ± 0.02 km s^{-1} (Carrera et al., in prep.). Because of the large velocity dispersion reported by *Gaia* and the discrepancy among the different radial velocity determinations, we consider it as a probable spectroscopic binary. None of these stars present doubling of their lines, and so the measure of the atmospheric parameters is negligibly affected by the presence of an unseen companion with respect to the precision of our analysis.

4. Stellar parameters

Atmospheric parameters were determined spectroscopically, minimising abundance trends with excitation potential and the strength of the line and imposing ionisation equilibrium. In this section we describe this procedure.

4.1. Line list and equivalent width measurement

We adopted the line list for Fe I from Ruffoni et al. (2014) and Fe II from Meléndez & Barbuy (2009), selecting the lines in the 430 to 640 nm interval. HARPS-N spectra start from 383 nm; however, the S/N is quite low in that region for our spectra. This

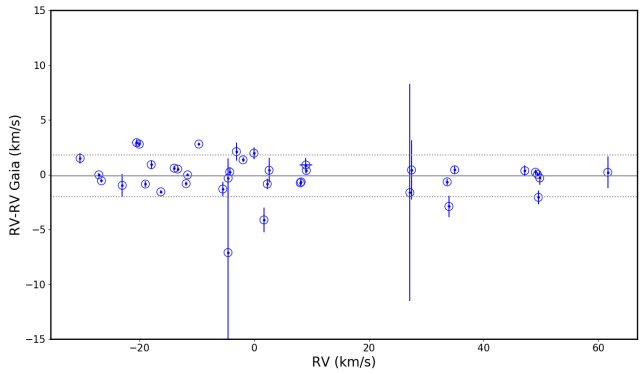

Fig. 3. Difference in radial velocities for targets between *Gaia* and this work. The error of our sample is shown on the x-axis (it is so small that it falls within the symbol), and only the *Gaia* error is plotted on the y-axis, as it is much larger. The grey lines indicate the mean value of offset -0.11 ± 1.9 km s^{-1} (standard deviation).

fact, combined with the extreme crowding of features in the blue part of the spectrum, led us to discard all Fe lines bluer than 430 nm, as their intensity could not be measured with the same accuracy as those in redder regions.

Equivalent widths (EWs) were measured with the code ARES, following the procedure described in Sousa et al. (2015), using a S/N-dependent approach to set the local continuum. Visual inspection was performed for very strong lines (EW > 150 mÅ) and lines with large fitting errors (EW < $3 \times \sigma$(EW)) and we performed a manual measurement of the EW using IRAF splot when the inspection showed an issue with the ARES fitting (e.g., incorrect continuum placing due to a badly subtracted cosmic ray). Lines which turned out to be blended were discarded.

4.2. Photometric parameters

The determination of the atmospheric parameters requires a set of initial parameters to be used in the first iteration of the abundance analysis determination. For this purpose, we used photometric parameters, that are determined on the basis of observed photometric colour(s) and the latest generation of stellar isochrones.

To determine the initial stellar effective temperature ($T_{\rm eff}$) we used IRFM (Infrared flux method). This method is model independent and relies on the flux on the stellar surface at IR wavelength which relates to the surface temperature. We derived the J–K colours from 2MASS, and applied the appropriate reddening for the target coordinate as derived from IRSA (Schlafly & Finkbeiner 2011). The computation of photometric surface temperature follows the colour-temperature polynomial fitting based on a sample of F0–K5 type from Alonso et al. (1999), appropriate for stars in the range 3700–5300 K, which is consistent with our sample.

To determine $\log g$ we used Padova CMD isochrones (PARSEC release v1.2s, Marigo et al. 2017 and COLIBRI, Pastorelli et al. 2020, and references therein), with web interface CMD 3.4.

For age and metallicity input for the isochrones we used information taken from the literature (see Table 1). In cases where no metallicity estimate was available, we adopted the average metallicity of the thin disc ([Fe/H] = −0.25 dex Soubiran et al. 2003). This is admittedly low for a typical OC, but has a negligible impact on the final parameters in Table 3.

Table 3. Initial parameters from photometric data.

Name	$T_{\rm eff}$ (K)	$\log g$ (dex)	[Fe/H] (dex)	$v_{\rm micro}$ (km s^{-1})
ASCC 11	4867	2.36	−0.25	1.0
Alessi 1_1	4677	2.39	−0.25	1.0
Alessi 1_2	4600	2.28	−0.25	1.0
Alessi 1_3	4804	3.50	−0.25	1.0
Alessi 1_4	4578	2.25	−0.25	1.0
Alessi-Teusch 11	4790	3.40	0.10	1.0
Basel 11b_1	6259	1.70	0.01	1.0
Basel 11b_2	5917	1.59	0.01	1.0
Basel 11b_3	5693	1.83	0.01	1.0
COIN-*Gaia* 30	5231	1.70	−0.25	1.0
Collinder 463_1	4730	2.12	−0.25	1.0
Collinder 463_2	4730	2.30	−0.25	1.0
Gulliver 18	4598	1.50	−0.25	1.0
Gulliver 24	4567	1.62	−0.25	1.0
Gulliver 37	5095	1.80	−0.25	1.0
NGC 2437_1	4792	2.24	0.00	1.0
NGC 2437_2	5218	3.38	0.00	1.0
NGC 2437_3	5206	3.38	0.00	1.0
NGC 2437_4	5087	2.39	0.00	1.0
NGC 2437_5	4990	2.37	0.00	1.0
NGC 2437_6	4848	2.29	0.00	1.0
NGC 2437_7	4549	1.95	0.00	1.0
NGC 2509	4705	2.27	0.00	1.0
NGC 2548_1	5114	2.50	−0.24	1.0
NGC 2548_2	5047	2.27	−0.24	1.0
NGC 2548_3	4853	2.35	−0.24	1.0
NGC 2548_4	5327	2.70	−0.24	1.0
NGC 7082	4994	1.56	−0.01	1.0
NGC 7209_1	4799	2.50	0.01	1.0
NGC 7209_2	4142	1.50	0.01	1.0
Tombaugh 5_1	5024	2.42	0.06	1.0
Tombaugh 5_2	5021	2.40	0.06	1.0
Tombaugh 5_3	5270	2.44	0.06	1.0
UPK 219	5203	3.01	−0.25	1.0
Comparison clusters				
Collinder 350_1	4200	1.30	0.10	1.0
Collinder 350_2	5300	3.20	0.10	1.0
NGC 2682_1	4537	3.61	0.00	1.0
NGC 2682_2	4601	2.50	0.00	1.0
NGC 2682_3	4823	2.90	0.00	1.0
NGC 2682_4	4967	3.36	0.00	1.0

We note that, while it is important to provide reasonably accurate input parameters in the isochrones to derive similarly reasonable photometric parameters, these values are simply a starting point from which to build the initial model atmosphere. The actual atmospheric parameters have been determined on the basis of the observed spectra (see following section).

4.3. Spectroscopic parameters

The atmospheric parameters analysis was performed using the code MOOG (used through the Python wrapper pymoogi[4], based on the MOOG 2019 version), a 1D, local thermodynamic equilibrium (LTE) stellar line analysis code. The model atmospheres

[4] https://github.com/madamow/pymoogi

Table 4. Mean RV and metallicity for the observed clusters.

Cluster	RV (km s^{-1})	σRV (km s^{-1})	[Fe/H] (dex)	σ[Fe/H] (dex)	N
ASCC 11	−10.94	0.19	−0.14	0.05	1
Alessi 1	−4.37	0.85	0.00	0.08	4
Alessi-Teusch 11	−27.11	0.12	−0.19	0.05	1
Basel 11b	2.17	0.37	−0.01	0.05	3
COIN-*Gaia* 30	−26.66	0.13	0.03	0.05	1
Collinder 463	−10.66	0.98	−0.15	0.05	2
Gulliver 18	−1.97	0.18	−0.10	0.05	1
Gulliver 24	−30.37	0.16	−0.10	0.05	1
Gulliver 37	−4.59 [(a)]	0.17	0.10	0.05	1
NGC 2437	49.13 [(a)]	0.93	0.00	0.04	7
NGC 2509	61.63	0.14	−0.10	0.06	1
NGC 2548	8.41 [(a)]	0.46	−0.02	0.03	4
NGC 7082	−11.89	0.15	−0.15	0.05	1
NGC 7209	−18.49	0.51	−0.04	0.04	2
Tombaugh 5	−21.21	1.30	0.05	0.05	3
UPK 219	−0.07	0.15	0.02	0.05	1
Comparison clusters					
Collinder 350	−15.14	1.16	0.00	0.05	1
NGC 2682	34.28 [(a)]	0;65	0.03	0.03	4

Notes. [(a)]Binary systems (see Table 2). When only 1 star is observed, σ is the error, nor the dispersion.

were calculated interpolating the ATLAS9 stellar atmosphere library (Castelli & Kurucz 2003) in 1D plane-parallel geometry. While in principle spherical models should be better for giants, in practice this choice does not introduce significant differences (see e.g., Casali et al. 2020).

Atmospheric parameters were determined iteratively, by varying their values in the input model atmosphere until excitation and ionisation equilibria were reached.

In other words, $T_{\rm eff}$ and microturbulent velocities ($v_{\rm micro}$) were determined by minimising the trends of Fe I abundance as determined from different lines as a function of their excitation potential and their intensity, respectively; surface gravity was determined by matching (within the errors) output Fe I and Fe II abundances. While we adopt the solar abundances from Grevesse & Sauval (1998), we also repeated the procedure for a solar spectrum collected with HARPS-N during one of our runs, finding an Fe abundance essentially identical to that reported by Grevesse & Sauval (1998). Errors on the atmospheric parameters were derived following the same procedure outlined in Epstein et al. (2010).

The resulting atmospheric parameters along with their associated uncertainties are reported in Table A.2 for all individual targets. The mean value of metallicity for each cluster is quoted in Table 4 (where, for Collinder 350, we use only the warmer star).

4.4. Comparison with literature

Two clusters, namely Collinder 350 and NGC 2682 (M67) have been included in the present sample for comparison. The former was investigated in a previous SPA paper (Casali et al. 2020), which reports results obtained with a slightly different approach for the same stars, therefore allowing the mapping of possible offsets. The latter, NGC 2682, is one of the most studied OCs and represents an ideal benchmark cluster. Some recently published analyses are available for a few more of the clusters in our sample. One of them was purposely observed (Tombaugh 5) as the existing spectra were of moderate resolution; for two others (Basel 11b, NGC 2548) the results were published after our observations had already been made. Finally, we note that some other clusters (ASCC 11, Alessi-Teusch 11, Collinder 350, NGC 2548, and NGC 2682) were observed within the LAMOST survey, at $R = 1800$ (Zhang et al. 2019). However, we do not discuss this last case, limiting comparisons only to spectra with at least moderate resolution ($R > 10\,000$).

We provide details below and briefly summarise how our results compare to the literature. In particular, Fig. 4 gives a visual comparison, while Table 5 presents detailed values for the benchmark cluster NGC 2682 and the other stars. We note that for NGC 2682, there are no systematic differences among the different studies.

Collinder 350. In our sample, we collected and analysed spectra for two members of Collinder 350, one of the least studied open clusters in the solar neighbourhood. For the coolest star (4200 K) we obtained [Fe/H] = −0.40 ± 0.08 dex, while for the hottest (5300 K) we found [Fe/H] = 0.00 ± 0.05 dex. In the work of Blanco-Cuaresma & Fraix-Burnet (2018), the metallicity was estimated at 0.03 dex from the spectrum of one single star with a resolution about 80 000. In the SPA paper by Casali et al. (2020), the value of [Fe/H] was measured using two methods on the same stars as in our analysis. Even in this case the two stars show a difference in the measured metallicity, albeit smaller than in the present analysis. With ROTFIT (i.e. fitting of spectral libraries) these latter authors found 0.03 ± 0.07 dex (cooler star) and −0.02 ± 0.09 dex (hotter star) while with FAMA (i.e., automatic method based on EWs analysis) they derive −0.24 ± 0.02 dex (cooler star) and −0.03 ± 0.06 dex (hotter star).

Our result are in fair agreement. overall with the literature, The hottest star shows [Fe/H] = 0, a value consistent with that from both methods used by Casali et al. For the coolest star, our result is more metal poor than that measured by these latter authors using either of the method stated above. As mentioned by Casali et al. (2020), we believe that at such temperature the placement of the continuum is challenging for these stars, as they are very rich in absorption lines, which leads to less accurate metallicities for stars with low temperatures ($T_{\rm eff} < 4300$ K, $\log g < 1.8$ dex).

NGC 2682 (M67). This is one of the most studied open clusters, and solar metallicity and age information are available (see e.g., Bertelli Motta et al. 2018; Bossini et al. 2019). We observed four stars, two single stars on the red clump, and two red giants known to be binary systems (see Tables 2 and 5). In particular, the two single-lined binaries (stars numbered 3 and 4 in our list) were studied by Mermilliod et al. (2007, 2008) and Geller et al. (2021), who derived their orbital parameters. Star NGC 2682 3 (aka S1237) is a yellow straggler (Leiner et al. 2016),that is,a star falling between the blue stragglers (BSS) and the red giants, above the subgiant branch level in optical CMDs. Leiner et al. (2016) used *Kepler* K2 data to derive a mass of 2.9 ± 0.2 $M_{\odot}$, about twice the mass of turn-off stars, corroborating the notion that yellow stragglers are a later evolutionary phase of BSS. We collected results of spectral analyses from multiple studies and list them in Table 5. The parameters are in good agreement with the literature overall.

Tombaugh 5. A metallicity estimate based on moderate-resolution spectroscopy also exists for Tombaugh 5. Baratella et al. (2018) reported atmospheric parameters (from mid-resolution spectra, $R = 13\,000$) for five members out of

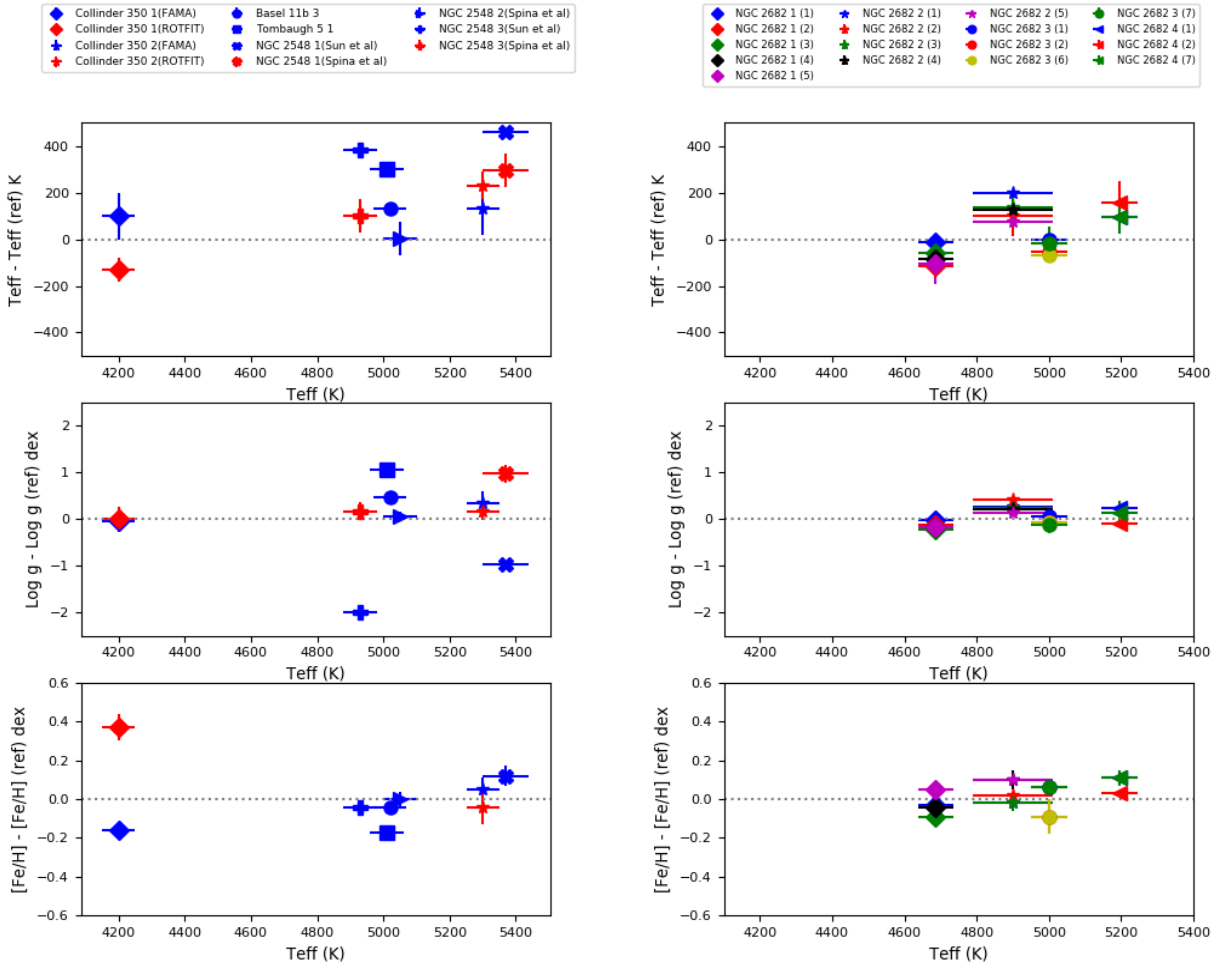

Fig. 4. Comparison of atmospheric parameters for targets with high resolution spectroscopic determinations. We plot out $T_{\rm eff}$ in the x axis and the difference (our minus literature) and the error from literature on the y-axis. In the *right column* we show the different sources in NGC 2682 and in the *left column* all other clusters. Ref: (1) Jacobson et al. (2011); (2) APOGEE DR16; (3) (Casamiquela et al. 2017) EW; (4) Casamiquela et al. (2017) SS; (5) Gao et al. (2018); (6) Luck (2015);(7) Spina et al. (2021).

seven observed. In this case two stars are in common with our sample; we targeted them for this reason. However, only one (Tombaugh 5_1 for us, 7701 in Baratella et al. 2018) is analysed in both papers, as they considered the second (Tombaugh 5_2 for us, 8099 in Baratella et al. 2018) to be a possible non-member on the basis of its RV and previous literature. The latter star has a high probability of being a member according to Cantat-Gaudin et al. (2018b) and the RVs measured by us and *Gaia* RVS support its membership. Baratella et al. (2018) derived temperature and gravity spectroscopically and measured abundances using EWs, with estimated errors of 0.15–0.20 dex. These authors found an average metallicity of 0.06 ± 0.11 dex. The mean value from our analysis is 0.05 ± 0.05 dex. The agreement between the analyses for all atmospheric parameters is reasonable given the large difference in resolution between the data sets (see Fig. 4).

NGC 2548. A recent paper Sun et al. (2020) is based on moderate-resolution spectra. These latter authors report the radial and rotational velocities for nearly 300 stars in NGC 2548 (M48), measured with Hydra@WIYN spectra ($R \sim 135\,00$) in a region of about 40 nm in width around the Li I 670.8 nm line. The candidate cluster stars were selected from CMDs based on UBVRI photometry and, based on a combination of spectroscopic data and *Gaia* DR2 results, about two-thirds of them turned out to be members-both single and in binary/multiple systems. Temperature and gravity were derived from photometric data. For a subsample of 99 well-behaved, low-rotational-velocity, single cluster members, the value of the metallicity was derived using 16 Fe I lines, finding an average metallicity $[\mathrm{Fe/H}] = -0.06 \pm 0.007$ dex. This is in agreement with our finding of -0.02 ± 0.04 dex from four stars in our sample.

Two stars are in common with our sample, for which Sun et al. (2020) report $T_{\rm eff}$ of 4912 K and 4549 K, with $\log g$ 4.64 and 4.69 respectively. We obtain $T_{\rm eff}$5370 ± 110 K and 4930 ± 60 K and our values for $\log g$ are much lower, 3.67 ± 0.1 dex and 2.68 ± 0.05 dex respectively, consistent with the stars being evolved rather than on the main sequence. The gravities in Sun et al. (2020) were derived using the Yale-Yonsei isochrones, an approach that leads to two possible solutions, corresponding to an evolved or a main sequence star. Sun et al. (2020) adopted the dwarf solution, and the reason for this choice is not discussed in the paper. However, given the positions of the observed stars on the CMD (see Fig. 2), we expect that the solution corresponding to an evolved (and thus brighter) star is the most appropriate one.

Basel 11b. Finally, among the 128 OCs published in Donor et al. (2020) and based on SDSS/APOGEE DR16, there is Basel_11b. The paper presents the metallicity based on one

Table 5. Comparison of atmospheric parameters with literature.

Star	$T_{\rm eff}$ (K)	$\sigma T_{\rm eff}$	log g (dex)	σlog g	[Fe/H] (dex)	σ[Fe/H]	Reference	Notes
NGC 2682_1	4687	50	2.37	0.07	−0.05	0.05	Present study	RC, single
	4700		2.40		−0.02		Jacobson et al. (2011)	
	4803	84	2.48	0.04		0.01	APOGEE DR16	
	4745	57	2.59	0.09	0.04	0.04	Casamiquela et al. (2017) EW	
	4771	13	2.55	0.03	−0.04	0.05	Casamiquela et al. (2017) SS	
	4793		2.55		−0.10		Gao et al. (2018)	
NGC 2682_2	4900	110	2.76	0.10	0.02	0.05	Present study	RC, single
	4700		2.50		0.04		Jacobson et al. (2011)	
	4802	84	2.34	0.04	0.00	0.01	APOGEE DR16	
	4762	37	2.53	0.07	0.04	0.04	Casamiquela et al. (2017) EW	
	4776	13	2.54	0.03	−0.08	0.05	Casamiquela et al. (2017) SS	
	4824		2.62		−0.08		Gao et al. (2018)	
NGC 2682_3	5000	50	2.77	0.10	−0.03	0.03	Present study	SB1, $P \sim 700^d$ (Geller et al. 2021),
	5000		2.70		−0.09		Jacobson et al. (2011)	Yellow straggler (Leiner et al. 2016)
	5056		2.85		0.06	0.09	APOGEE DR16	
	5067		2.85		0.06	0.09	Luck (2015)	
	5018	71	2.88	0.19	−0.09	0.04	Spina et al. (2021)	
NGC 2682_4	5195	50	3.25	0.10	0.00	0.05	Present study	SB1, $P \sim 43^d$ (Mermilliod et al. 2007;
	5100		3.00		−0.11		Jacobson et al. (2011)	Geller et al. 2021)
	5040	92	3.34	0.06	−0.03	0.01	APOGEE DR16	
	5098	71	3.12	0.26	−0.11	0.04	Spina et al. (2021)	
Collinder 350_1	4200	50	1.30	0.20	−0.40	0.08	Present study	
	4100	100	1.35	0.23	−0.24	0.01	Casali et al. (2020) FAMA	
	4330	50	1.28	0.24	−0.03	0.07	Casali et al. (2020) ROTFIT	
Collinder 350_2	5300	50	3.15	0.10	0.02	0.05	Present study	
	5170	110	2.85	0.27	−0.03	0.06	Casali et al. (2020) FAMA	
	5070	60	2.99	0.19	−0.02	0.09	Casali et al. (2020) ROTFIT	
Basel 11b_3	4950	50	2.83	0.10	−0.04	0.05	Present study	
	4817	86	2.37	0.04	0.00	0.01	APOGEE DR 16	2M05581816+2158437
Tombaugh 5_1	5010	50	3.17	0.15	0.04	0.05	Present study	
	4710		2.10		0.21	0.05	Baratella et al. (2018)	
NGC 2548_1	5370	70	3.67	0.15	0.00	0.05	Present study	
	4912		4.64				Sun et al. (2020)	
	5074	73	2.69	0.19	−0.12	0.05	Spina et al. (2021)	
NGC 2548_2	5050	50	2.65	0.10	−0.02	0.04	Present study	
	5049	72	2.59	0.10	−0.02	0.04	Spina et al. (2021)	
NGC 2548_3	4930	50	2.70	0.10	−0.01	0.05	Present study	
	4549		4.69				Sun et al. (2020)	
	4829	72	2.53	0.19	0.03	0.04	Spina et al. (2021)	

Notes. σ [Fe/H] is the error from metallicity measurement for present study; EW is the result obtained by the equivalent widths-based GALA software; SS is the results obtained from spectral synthesis using iSpec.

single star, [Fe/H] = 0. For this star we determined [Fe/H] = −0.04 and the mean iron abundance, based on three stars, is of −0.013 ± 0.034 dex. A futher comparison of the atmospheric parameters is found in Table 5.

5. Discussion

The average metallicities for our sample of OCs are given in Table 4. These are combined with the clusters positions in the following (Galactocentric distance and height on the plane) to discuss the metallicity distribution in the disc, adding literature data to increase the sample and the coverage of disc properties.

5.1. Metallicity distribution in the disc

The study of the radial and vertical fossil gradients such as age and composition is one of the main approaches in probing the Galactic disc(s).

In this section, we discuss the observed behaviour of OC metallicity, age and Galactocentric distance and the information that can be gained from a comparison with models for the disc. First we derive the classical radial gradient in metallicity (e.g., Friel et al. 2002) and then we compare observations with models. Our sample is distributed mostly on the Galactic plane, the SPA clusters are all within 0.5 kpc (Cantat-Gaudin et al. 2020), and are generally in the solar neighbourhood, with Galactocentric distance ranging between 7.7 and ∼10 kpc. With one single exception – NGC 2682, which was observed for comparison purposes – the clusters are relatively young, with 14 out of 18 clusters being younger than 0.5 Gyr.

By combining our data with results from some selected surveys and studies, we can widen the sample to older clusters and/or those at greater distances from the Galactic centre, building a sample that allows us to probe the properties of the Galactic disc, and can be used to constrain models of the chemo-dynamical evolution of the disc. The SPA sample currently includes the present analysis as well as four more OCs in

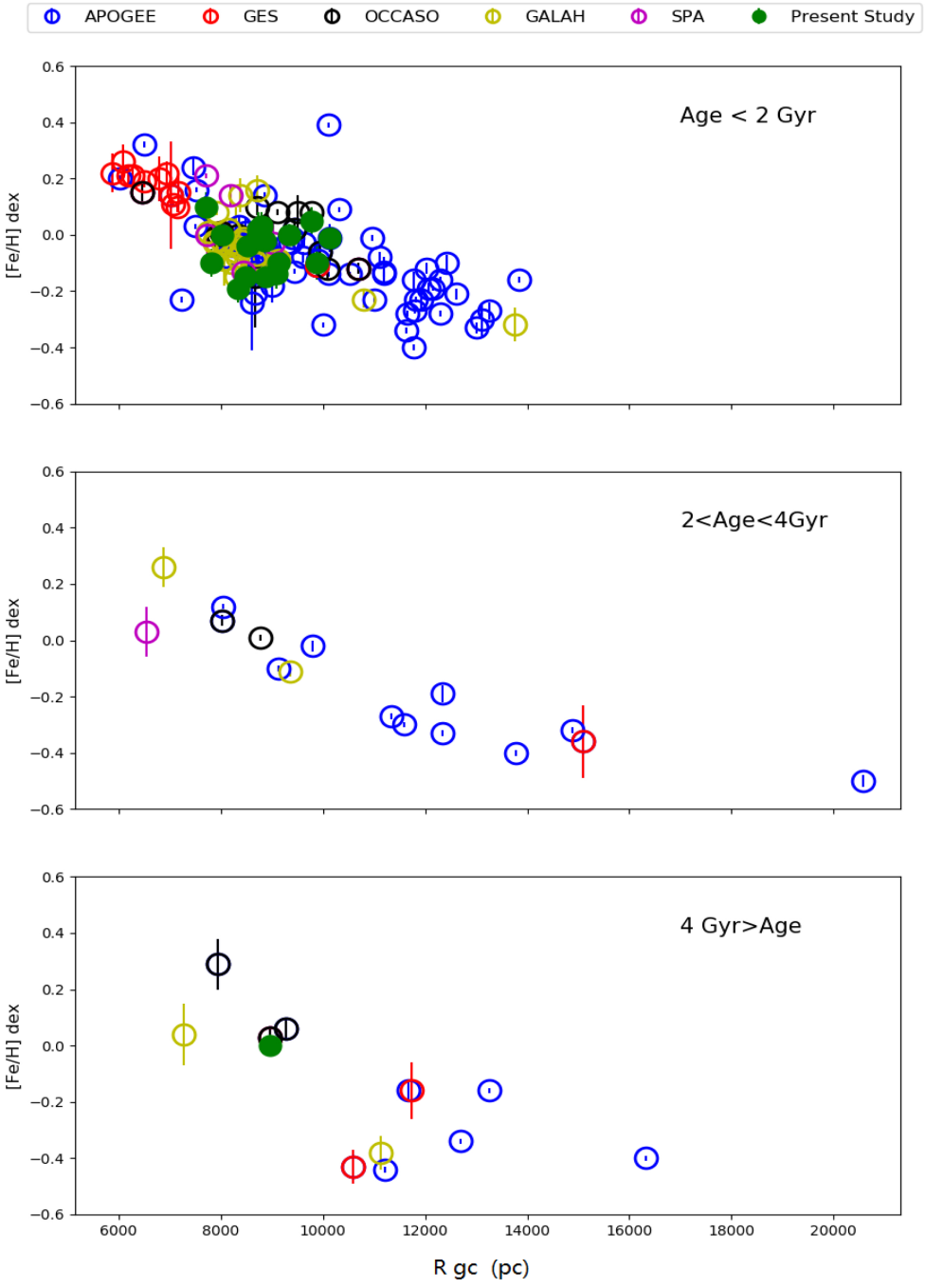

Fig. 5. Distribution of metallicity with Galactocentric distance in three age bins (the same used in Minchev et al. 2014a, see Sect. 5.2). In addition to our clusters, we show data from APOGEE (Donor et al. 2020), GES (Casali et al. 2019), OCCASO (Casamiquela et al. 2017), and GALAH (Spina et al. 2021) plus SPA results that have already been published (Frasca et al. 2019; Casali et al. 2020; D'Orazi et al. 2020).

Casali et al. (2020), one from D'Orazi et al. (2020), and another one in Frasca et al. (2019). We include the results from the large spectoscopic surveys, namely: (a) APOGEE[5] (Donor et al. 2020), with more than 120 OCs mostly in the 6–15 kpc range in R_{gc} and with [Fe/H] from −0.5 to 0.4 dex; (b) GES, covering the wide range of Galactocentric distance from 5.8 to 20 kpc, and the metallicity range −0.5 to 0.4 dex; and(c) GALAH (Spina et al. 2021), keeping only clusters whose parameters are based on HERMES spectra and excluding those based on the recalibration of APOGEE (see Spina et al. 2021 for details). Moreover, we include the OCCASO sample (Casamiquela et al. 2017), whose OCs are located at Galactocentric distances similar to those of the SPA project (6.5 to 10.5 kpc) and with metallicities around the solar value, ranging from −0.1 dex to 0.17 dex.

The relationship between metallicity and Galactocentric distance, classically referred to as the metallicity gradient, is shown

Table 6. Observed slope of the metallicity gradient.

Age (Gyr)	R_{gc} (kpc)	d[Fe/H]/dR_{GC} (dex kpc^{-1})	d[Fe/H]/d|z|$_{GC}$	$N_{clusters}$
All ages	Rgc < 14	−0.066 ± 0.005	−0.249 ± 0.062	157
All ages	Rgc > 14	−0.032 ± 0.007	−0.040 ± 0.028	4
Age < 2	Rcg < 14	−0.059 ± 0.006	−0.236 ± 0.119	133
2 < age < 4	Rgc < 14	−0.089 ± 0.007	−0.195 ± 0.144	13
Age > 4	Rgc < 14	0.008 ± 0.041	0.081 ± 0.117	11

[5] We downloaded the Value Added Catalog for the Open Clusters Chemical Abundance and Mapping project (OCCAM), at https://data.sdss.org/sas/dr16/apogee/vac/apogee-occam/

Table 7. Slope of the metallicity gradient from selected literature papers.

Reference	Sample	d[Fe/H]/dR_{gc}	N OCs	Comment
Friel et al. (2002)	Low-res optical spectra	−0.059 ± 0.010	39	$7 < R_{gc} < 16$ kpc, All ages [(a)]
Reddy et al. (2016)	High-res optical spectra	−0.052 ± 0.011	67	$6 < R_{gc} < 12$ kpc and $\|z\| < 500$ pc
		−0.015 ± 0.007	12	$12 < R_{gc} > 24$ kpc [(b)]
Carrera et al. (2019)	APOGEE DR14, GALAH DR2	−0.052 ± 0.003	46	$6 < R_{gc} < 13$ kpc [(c)]
		−0.077 ± 0.007		$6 < R_{gc} < 11$ kpc [(c)]
		0.018 ± 0.009		$11 < R_{gc} < 13$ kpc [(c)]
Casamiquela et al. (2019)	High-res optical spectra	−0.056 ± 0.011	18	$R_{gc} < 12$ kpc, All ages [(d)]
Donor et al. (2020)	APOGEE DR16	−0.068±0.004	68	$R_{gc} < 13.9$ kpc, all ages[(e)]
		−0.009 ± 0.011	3	$R_{gc} > 13.9$ kpc, All ages

Notes. [(a)]The slope is also given in different age ranges, with a gradient steepening for increased age: −0.023, −0.053, −0.075 for age <2, 2–4, and >4 Gyr, respectively (a similar result was found by Andreuzzi et al. (2011) using [Fe/H] from high resolution spectroscopy, who found values of −0.07 and −0.15 for age lower and larger than 4 Gyr, respectively). [(b)]They do not consider it representative of the disc midplane (their Sect. 5). [(c)]The first value is obtained for OCs where at least 4 stars were measured, the second and third to the whole sample. The gradient in the outer bin becomes −0.04 ± 0.01 if the two low metallicity OCs close to R_{gc}11 kpc are excluded. [(d)]No significant difference in the age ranges covered. [(e)]Also divided for age: −0.50 (13 OCs, age < 0.4 Gyr), −0.073 (16 OCs, 0.4–9,7 Gyr), −0.066 (27 OCs, 0.8–2 Gyr), and −0.094 (12 OCs, >2 Gyr).

in Fig. 5 for the combined sample, dividing it into three age intervals (selected because they are the same in Minchev et al. 2014a, see below). The metallicities come from the cited sources (averaging values when more than one was available for a given cluster) and the R_{gc} values come from Cantat-Gaudin et al. (2020) where $R_{gc,Sun} = 8.34$ form Reid et al. (2014). Table 6 contains the corresponding gradients for the whole sample and separated into age bins. As the slope shows a change at about $R_{gc} = 14$ kpc, we use that limit to distinguish inner from outer regions. The same was done in past works, as can be seen from Table 7, where we list some selected literature. We show the values in Friel et al. (2002), because this is possibly the first analysis of a homogeneous and large spectroscopic sample, albeit based on low- resolution spectra, and in a few recent papers. As every work uses different age bins and R_{gc} ranges, we can make only a qualitative assessment of the results. However, the values in the two tables compare generally well; a few discrepant values are mentioned in the notes of Table 7.

Figure 6 shows metallicity as a function of distance from the Galactic plane, divided into age bin as in the previous figure. The calculated values are listed in Table 6 as well. We note that, overall, the trend with $|z|$, even in well-populated bins (e.g., young clusters in the inner disc), are far less statistically relevant than the corresponding slope with respect to Galactic radius.

We also explored possible residual azimuthal gradient (only for well-populated bins), finding extremely weak and moderately significant trends. For the overall sample within 14 kpc, we find 0.0028 ± 0.0007, while for the sample below 2 Gyr within the same radius we find 0.0022 ± 0.0009.

5.2. Comparison with chemo-dynamical models

It must be kept in mind that the chemo-dynamical evolution of the Galactic disc(s) is a rather complex process and the expectation is that much of the initial information will be diluted through the dynamical evolution and radial mixing of the disc. However, the effect of this are expected to differ depending on the age of the population: broadly speaking, the older a cluster is, the more it has undergone dynamical evolution and radial mixing, even if other factors come into play, such as the details of the formation environment and, more generally, the shape and mass of the disc at the time of formation and early evolution.

Recent models for the Galactic thin disc, such as those Minchev et al. (2013, 2014b,a), taking into account sophisticated simulations in the cosmological context (Martig et al. 2009, 2012) along with detailed knowledge of the chemical evolution of the disc, have been able to generate theoretical gradients to compare with the observations at different ages. However, uncertainties also exist due to model assumptions (e.g., initial gradient of chemical abundance), especially with regard to the oldest clusters and those furthest from the Galactic plane, which have undergone a large amount of dynamical evolution during their lives.

Minchev et al. (2014b) provide gradients calculated for different age intervals and ranges of distance from the Galactic plane. Figure 7 shows the comparison between the combined sample predictions from the chemo-dynamical thin-disc model by (the so-called MCM model Minchev et al. 2014a). Such models are calculated taking into account cosmological and dynamical properties, and chemical evolution, combining the effects of migration, the distance above the disc midplane, and then extending the model beyond the solar neighbourhood. Furthermore, the uncertainties on observation, and the evolution of Galactic disc were considered. From the MCM models we consider the range 0–0.8 kpc in terms of distance from the Galactic plane, which is appropriate for clusters in SPA, but also for the vast majority of the cluster samples from the literature. We plot the predictions for both $|z| < 0.3$ kpc and for 0.3 kpc< $|z|$ <0.8 kpc.

Figures 7 and 8 show comparisons between MCM predictions and results from observational data, grouped according to age in bins of 0.3 and 0.5 Gyr, respectively, up to 4.5 Gyr. Predictions generally show a good match to observations in the age range from 0.3 Gyr to 4.5 Gyr. It is worth noting that in the oldest age bin, two of the three discrepant clusters have $|z| > 1$ kpc, which is larger than the range the models have been calculated for, while the third has a metallicity based on one single star. On the other hand, bin the fitting is very poor in the youngest, even if the clusters lie closer than 0.5 kpc from the Galactic plane; we return to this problem below. For a more quantitative comparison with the Minchev et al. (2014a) results we derived

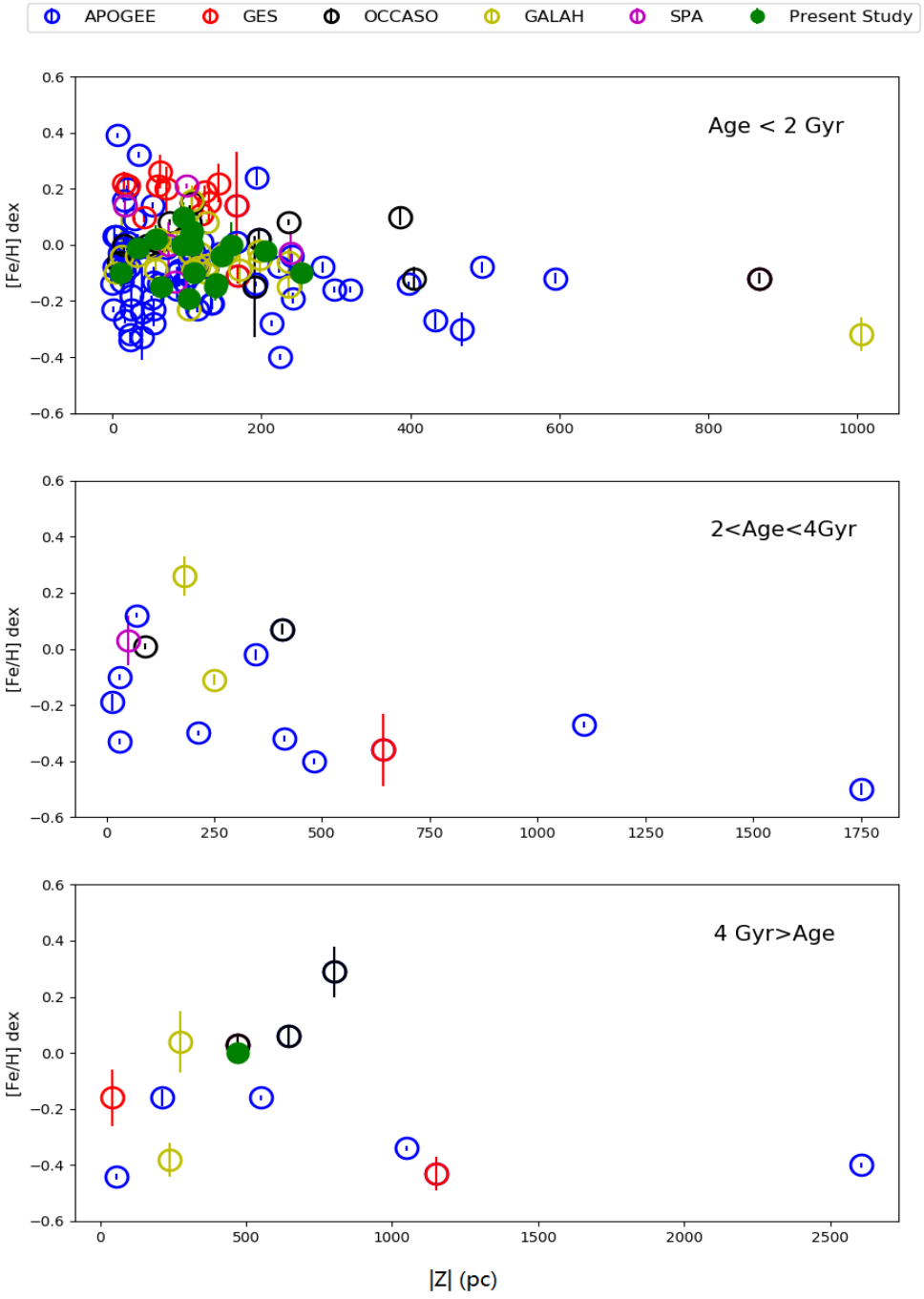

Fig. 6. Distribution of metallicity with distance from the midplate in three age bins (the same used in Minchev et al. 2014a, see Sect. 5.2). In addition to our clusters, we show data from APOGEE (Donor et al. 2020), GES (Casali et al. 2019), OCCASO (Casamiquela et al. 2017), and GALAH (Spina et al. 2021) plus SPA results that have already been published (Frasca et al. 2019; Casali et al. 2020; D'Orazi et al. 2020).

the gradients in our sample following the bins in age and Z in their Table 1, considering the error on metallicities in the fitting process. We employed the same separations in R_{gc} and $|z|$ as these latter authors and computed the corresponding gradients for the observed sample. Interestingly, the gradient computed for age younger than 2 Gyr and $|z| < 0.25$ kpc, that is, the bin comprising the vast majority of our sample (97 OCs), is comparable to that from the prediction: -0.066 ± 0.008 versus -0.057 for observed and predicted slope, respectively (However, see below, for a caveat on the very young clusters). Values are instead different in the other bins, which are, nevertheless, very scarcely populated, and so it is difficult to assess if the discrepancy is important.

Coming back to the very different distribution of OC metallicity for young ages (already noted in previous studies e.g., Spina et al. 2017), several possible factors might be the source(s) of the poor fit. On the observational side, inaccurate measurements of the parameters could be the cause. For example, systematic underestimation of the Galactic distances would lead to outer disc clusters being compared to solar neighbourhood predictions. Systematic underestimation of Z, on the other hand, would mean that we were using predictions that are unsuitable for the sample. R_{gc} and Z are based on *Gaia* DR2 data, with typical uncertainties of around 5% to 10% on distance (Cantat-Gaudin et al. 2020), which is not large enough to generate the observed effect. Moreover, if such systematic errors existed, they would very likely affect clusters in the other age bins similarly, a phenomenon for which there is no evidence. We note that a systematic error in the adopted age could not in any way explain the poor fit: the discrepant clusters with <0.3 Gyr

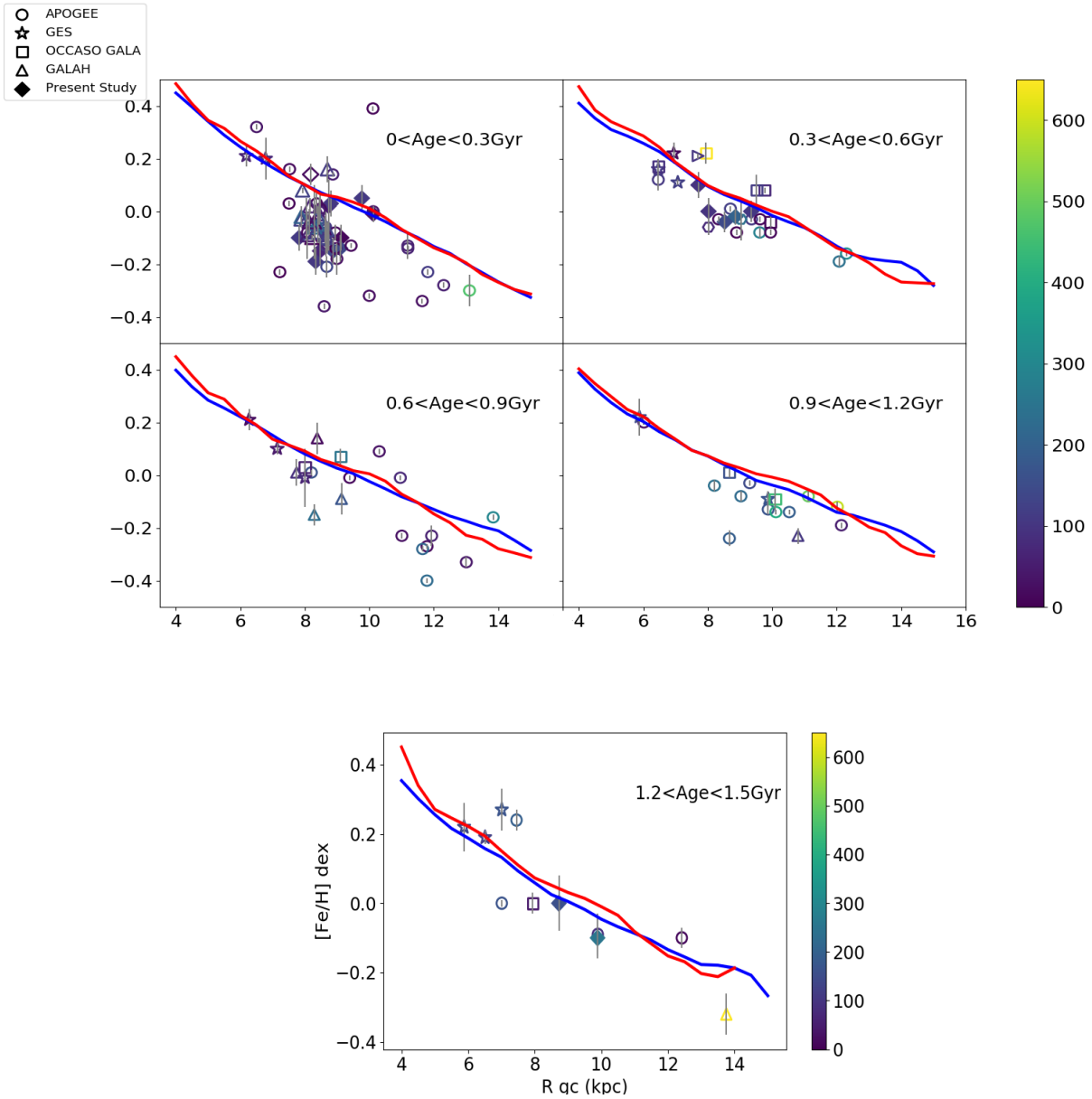

Fig. 7. Comparison between model predictions (Minchev et al. 2014a,b) and observations for young clusters. The red and blue lines are predictions from the MCM models for $|z| < 0.3$ kpc and $0.3 < |z| < 0.8$ kpc respectively. The colour of shading in the symbols indicates the distance from the Galactic plane. All considered clusters are within 0.6 kpc from the Galactic plane, with SPA clusters all being within 0.5 kpc. The open diamond in the first panel is ASCC 123 (Frasca et al. 2019) and the triangle symbol in the 0.3–0.6 Gyr range is NGC 2632 (D'Orazi et al. 2020) The fit is generally good for clusters older than 0.3 Gyr, but the predictions fail to reproduce the data among the very young clusters (see text).

would not be reproduced by predictions of any of the plotted ages.

Another possibility is that (some of) the metallicities we are using in the plot are not sufficiently accurate. In particular, we checked the APOGEE cluster from Donor et al. (2020) in more detail. Firstly, we detect hat for several clusters there are significant differences between the two latest data releases, DR16 (Donor et al. 2020) and DR14 (Donor et al. 2018; Carrera et al. 2019), even if the same stars are used in both cases. This is for instance the case of King 7, with $[Fe/H] = -0.13 \pm 0.05$ and -0.04 ± 0.01 in DR16 and DR14, respectively. These differences may be explained by the different methodologies used in the two releases to obtain the final abundances (see Jönsson et al. 2018, 2020, for a detailed explanation). For several clusters the values are based on a single star with either low astrometric membership probability from Cantat-Gaudin et al. (2018b) (e.g., Berkeley 79, Czernik 23, FSR 852, King 12, and NGC 1857) and/or with discrepant radial velocities in comparison with the literature, e.g., Czernik 23, NGC 2311, NGC 6383. Additionally, the star observed in NGC 2311 lies well outside the cluster sequence and the star in NGC 6383 has a high rotation velocity (>20 km s^{-1}) which complicates its analysis. In principle the APOGEE sample includes two stars in NGC 2232 with atmospheric parameters akin to those of giant, but this cluster does not contain giants. Moreover, they have a negligible astrometric membership probability from Cantat-Gaudin et al. (2018b) and their radial velocities (~82 km s^{-1}) are in disagreement with the average value derived from 19 stars (~25 km s^{-1}) with very high astrometric probabilities from *Gaia* DR2 by Soubiran et al. (2018). In the case of the star forming region NGC 1977,

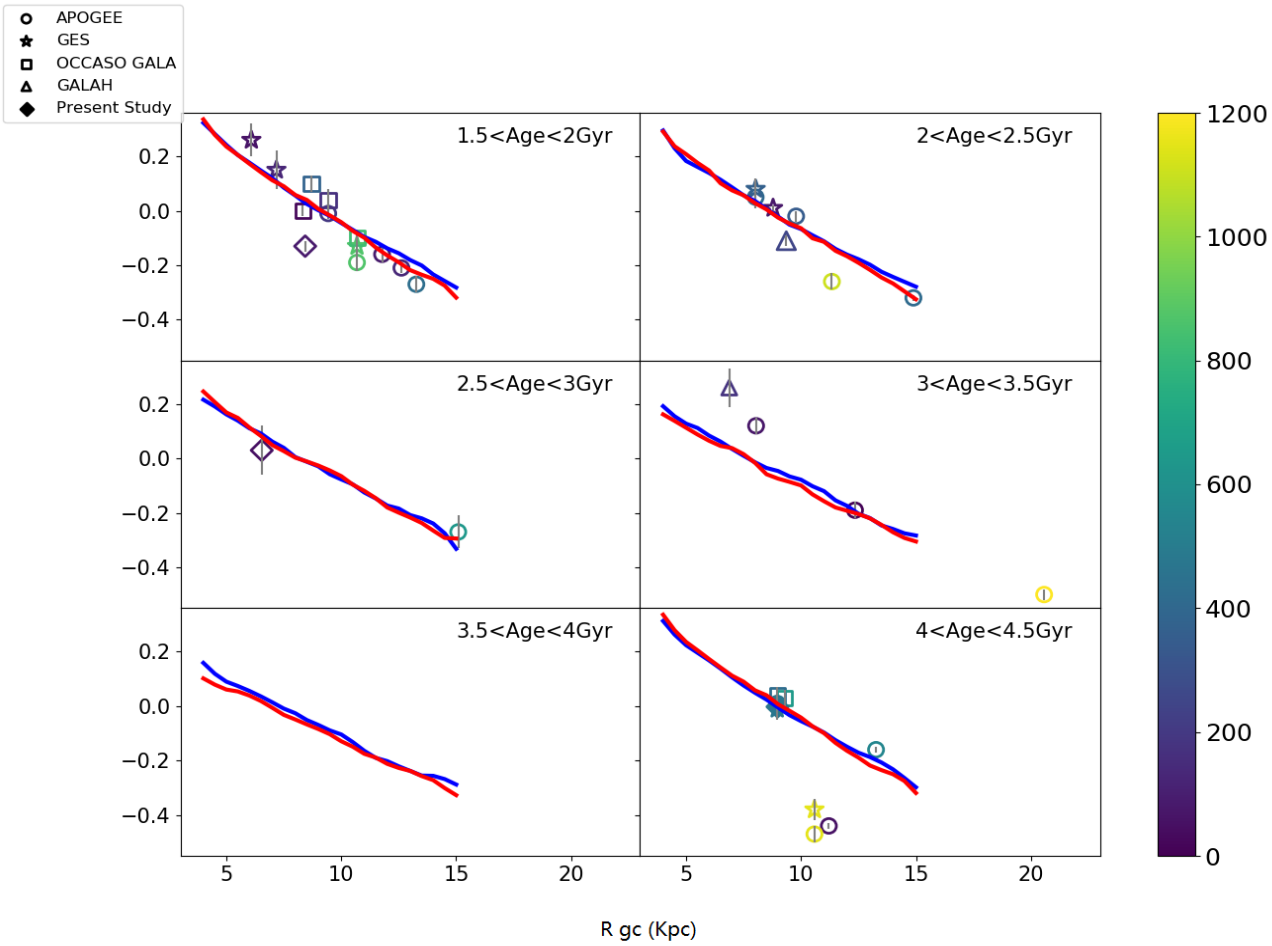

Fig. 8. As in Fig. 7 but for clusters of bewteen 1.5 and 4.5 Gyr in age. We note the paucity of OCs older than 2.5 Gyr (in particular, only one SPA cluster is present, Ruprecth 171, from Casali et al. 2020). The data are quite well reproduced by the models; the exceptions are the old and very metal-poor clusters that have $|z| > 1$ kpc, further away from the Galactic plane than the plotted models.

the DR16 metallicity of [Fe/H] = −0.21 dex, derived from three stars (there is no determination in DR14) is in disagreement with the value reported from high-quality high-resolution spectroscopy by Netopil et al. (2016) of [Fe/H] = −0.06 dex from two stars obtained from Cunha et al. (1995). In the case of NGC 2264, again without astrometric membership probabilities available there is good agreement between APOGEE DR16 ([Fe/H] = −0.18 dex from 23 stars) and the value determined by King et al. (2000) ([Fe/H] = −0.18 dex from three stars) but they disagree with the recent determination by Baratella et al. (2020a) of [Fe/H] = +0.11 dex from a single star observed with UVES as part of *Gaia*-ESO. Baratella et al. (2020a) amply discusses the problems faced in analysing spectra of MS stars in samples of young stars and try to devise a more robust method. In contrast, there are other cases, such as Berkeley 33, NGC 136, and SAI 116, whose metallicities seem reliable although they are based on only 4, 1 and 2 stars, respectively. These stars have a very high astrometric membership probability according to Cantat-Gaudin et al. (2018b) and the derived radial velocities are in good agreement with other values reported in the literature.

All these cases seem to indicate that we have to take the metallicity of young clusters with caution. We also tried to understand which ages are the most problematic. We show in Fig. 9 only clusters younger than 300 Myr, where symbol size is proportional to the number of stars available in each cluster. We find that sample size dose not appear to be the (main) source of the problem.

The clusters showing the larger discrepancies with respect to the model are younger than 200 Myr, and especially younger than 100 Myr. This affects analyses carried out in both the optical and the IR. As already discussed in the literature (Yana Galarza et al. 2019; Baratella et al. 2020b; Spina et al. 2020), chromospheric effects and considerable magnetic fields are at play in young dwarfs, making a traditional 1D LTE analysis based on minimising trends for Fe lines less than optimal. Moreover, an intensification of strong absorption lines those forming near the top of the stellar photosphere where the magnetic fields are more vigorous has been observed as a function of the activity level during the stellar cycle (Yana Galarza et al. 2019; Spina et al. 2020). The cause of this effect can be ascribed to Zeeman broadening of atomic lines or the effect of cool stellar spots. However, it is possible that many other phenomena related to the chromospheric activity, and neglected in stellar models, are simultaneously at work in contributing to this spectral variability. Interestingly, these problems for young stars have almost only been studied and discussed in the case of MS and PMS stars. Our sample clearly illustrates for the first time that the effect(s) also extend to giants. Indeed, this is not surprising, as the challenges posed by the modelaling of atmospheres and spectra for giants are even more severe than those for dwarfs.

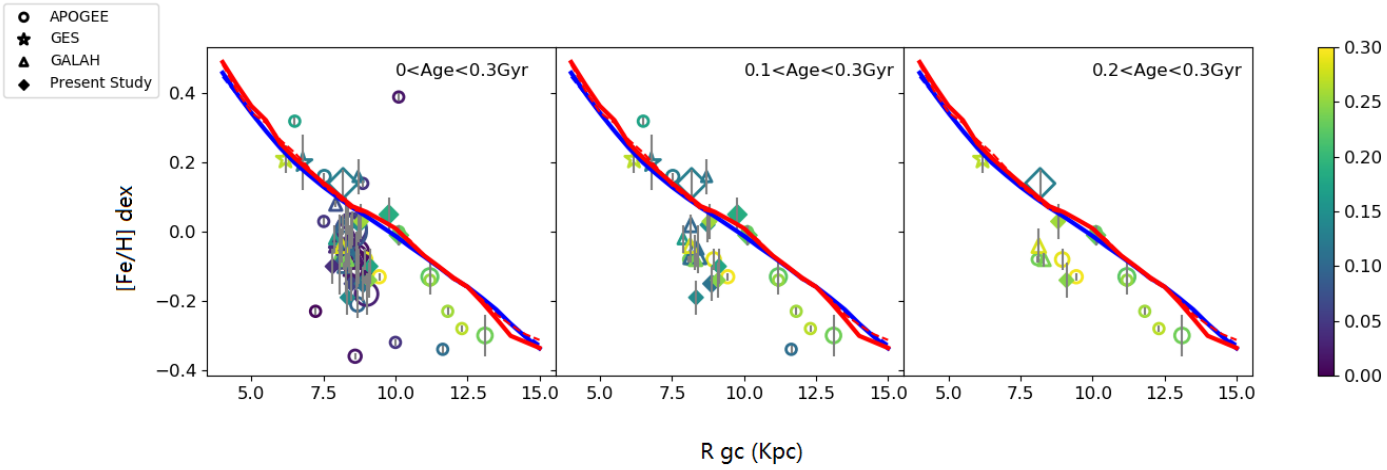

Fig. 9. As in Fig. 5, but with symbols colour-coded according to age. The size of the symbols is proportional to the number of stars studied in the cluster to obtain the mean value reported here. The open diamond represents ASCC 123 from Frasca et al. (2019). *Left panel*: all the clusters younger than 300 Myr, *middle and right panels*: fit without clusters younger than 100 Myr and 200 Myr, respectively. The fit to the models is quite reasonable when considering clusters older than 200 Myr.

6. Summary

This paper provides the atmospherical parameters for 40 red giants and red clumps in 18 OCs covering the Galactocentric distance range $7.7 < R_{gc} < 10$ kpc. Almost all of them are young clusters, with 15 OCs between 40 and 600 Myr, two around 1.5 Gyr, and one (NGC 2682) at 4.2 Gyr. Their parameters were measured using very high-resolution, high-S/N HARPS-N spectra, the EW method and 1D-LTE atmosphere models. Our main results can be summarised as follows.

(i) We obtained very precise radial velocities with uncertainties of 0.05–0.25 km s^{-1}. The offset between our results and those from *Gaia* DR2 is -0.11 ± 1.9 km s^{-1}.

(ii) Accurate stellar parameters were derived. For the stars located in the effective temperature range of 4200–5800 K uncertainties in T_{eff} are of around 60 K, and 0.12 dex in surface gravity. All of the clusters have metallicity close to solar, with a deviation within 0.05 dex.

(iii) We compared five of our clusters (Collinder 350, NGC 2682, Tombaugh 5, NGC 2548, Basel 11b) with results from previous work, finding no systematic bias in our determination. A few discrepant cases were examined.

(iv) We explored the trend between metallicities and Galactocentric distance combining our data with clusters from APOGEE, GES, OCCASO, GALAH, and other SPA OCs (ASCC 123, Gulliver 51, Ruprecht 171, NGC 2632, NGC 7044). We confirm the variation of slope in the metallicity gradient near $R_{gc} = 14$ kpc and find a gradient slope for the inner disc that is similar to that found in other, similar studies.

(v) We used the combined sample in a comparison with the chemo-dynamical predictions by Minchev et al. (2014b), finding good agreement for clusters older than 0.3 Gyr. Conversely, younger clusters show a large dispersion that is not predicted by models, with observed metallicities that are too low for the Galactocentric position (not explainable by radial mixing, given the young cluster age).

(vi) We examined the cases of young clusters with low metallicity, finding that some results may be doubtful. However, there seems to be a general difficulty in deriving accurate metallicities for clusters younger than about 200 Myr, both for dwarfs (confirming literature works) and giants. We tentatively ascribe this to the impropriety of the traditional analysis for young stars, as discussed in the previous section.

Acknowledgements. We thank the TNG personnel for help during the observations and I. Minchev for sharing his evolutionary models. This research used the facilities of the Italian Center for Astronomical Archive (IA2) operated by INAF at the Astronomical Observatory of Trieste. This work exploits the Simbad, Vizier, and NASA-ADS databases and the software TOPCAT (Taylor 2005). This work has made use of data from the European Space Agency (ESA) mission *Gaia* (`https://www.cosmos.esa.int/gaia`), processed by the *Gaia* Data Processing and Analysis Consortium (DPAC, `https://www.cosmos.esa.int/web/gaia/dpac/consortium`). Funding for the DPAC has been provided by national institutions, in particular the institutions participating in the *Gaia* Multilateral Agreement. We acknowledge funding from MIUR Premiale 2016 MITiC.

References

Alonso, A., Arribas, S., & Martínez-Roger, C. 1999, A&AS, 140, 261
Andreuzzi, G., Bragaglia, A., Tosi, M., et al. 2011, MNRAS, 412, 1265
Baratella, M., Carraro, G., D'Orazi, V., et al. 2018, AJ, 156, 244
Baratella, M., D'Orazi, V., Carraro, G., et al. 2020a, A&A, 634, A34
Baratella, M., D'Orazi, V., Biazzo, K., et al. 2020b, A&A, 640, A123
Bertelli Motta, C., Pasquali, A., Richer, J., et al. 2018, MNRAS, 478, 425
Blanco-Cuaresma, S., & Fraix-Burnet, D. 2018, A&A, 618, A65
Bossini, D., Vallenari, A., Bragaglia, A., et al. 2019, A&A, 623, A108
Cantat-Gaudin, T., Vallenari, A., Sordo, R., et al. 2018a, A&A, 615, A49
Cantat-Gaudin, T., Jordi, C., Vallenari, A., et al. 2018b, A&A, 618, A93
Cantat-Gaudin, T., Anders, F., Castro-Ginard, A., et al. 2020, A&A, 640, A1
Carrera, R., Bragaglia, A., Cantat-Gaudin, T., et al. 2019, A&A, 623, A80
Casali, G., Magrini, L., Tognelli, E., et al. 2019, A&A, 629, A62
Casali, G., Magrini, L., Frasca, A., et al. 2020, A&A, 643, A12
Casamiquela, L., Carrera, R., Blanco-Cuaresma, S., et al. 2017, MNRAS, 470, 4363
Casamiquela, L., Blanco-Cuaresma, S., Carrera, R., et al. 2019, MNRAS, 490, 1821
Castelli, F., & Kurucz, R. L. 2003, Model. Stellar Atmos., 210, A20
Castro-Ginard, A., Jordi, C., Luri, X., et al. 2019, A&A, 627, A35
Castro-Ginard, A., Jordi, C., Luri, X., et al. 2020, A&A, 635, A45
Carrera, R., & Pancino, E. 2011, A&A, 535, A30
Carrera, R., Bragaglia, A., Cantat-Gaudin, T., et al. 2019, A&A, 623, A80
Cunha, K., Smith, V. V., & Lambert, D. L. 1995, ApJ, 452, 634
Dalton, G., Trager, S., Abrams, D. C., et al. 2020, Proc. SPIE, 11447, 1144714
de Jong, R. S., Agertz, O., Berbel, A. A., et al. 2019, The Messenger, 175, 3
De Silva, G. M., Freeman, K. C., Bland-Hawthorn, J., et al. 2015, MNRAS, 449, 2604
Donor, J., Frinchaboy, P. M., Cunha, K., et al. 2018, AJ, 156, 142
Donor, J., Frinchaboy, P. M., Cunha, K., et al. 2020, AJ, 159, 199

D'Orazi, V., Oliva, E., Bragaglia, A., et al. 2020, A&A, 633, A38
Epstein, C. R., Johnson, J. A., Dong, S., et al. 2010, ApJ, 709, 447
Freeman, K., & Bland-Hawthorn, J. 2002, ARA&A, 40, 487
Friel, E. D., Janes, K. A., Tavarez, M., et al. 2002, AJ, 124, 2693
Frasca, A., Alonso-Santiago, J., Catanzaro, G., et al. 2019, A&A, 632, A16
Gao, X., Lind, K., Amarsi, A. M., et al. 2018, MNRAS, 481, 2666
Geller, A. M., Mathieu, R. D., Latham, D. W., et al. 2021, AJ, 161, 190
Gilmore, G., Randich, S., Asplund, M., et al. 2012, The Messenger, 147, 25
Girardi, L. 2016, ARA&A, 54, 95
Grevesse, N., & Sauval, A. J. 1998, Space Sci. Rev., 85, 161
Jacobson, H. R., Pilachowski, C. A., & Friel, E. D. 2011, AJ, 142, 59
Jeffries, R. D., Jackson, R. J., Cottaar, M., et al. 2014, A&A, 563, A94
Jönsson, H., Allende, Prieto C., Holtzman, J. A., et al. 2018, AJ, 156, 126
Jönsson, H., Holtzman, J. A., Allende, Prieto C., et al. 2020, AJ, 160, 120
Kharchenko, N. V., Piskunov, A. E., Schilbach, E., et al. 2013, A&A, 558, A53
King, J. R., Soderblom, D. R., Fischer, D., & Jones, B. F. 2000, ApJ, 533, 944
Lada, C. J., & Lada, E. A. 2003, ARA&A, 41, 57
Lagarde, N., Reylé, C., Robin, A. C., et al. 2019, A&A, 621, A24
Leiner, E., Mathieu, R. D., Stello, D., et al. 2016, ApJ, 832, L13
Liu, L., & Pang, X. 2019, ApJS, 245, 32
Luck, R. E. 2015, AJ, 150, 88
Majewski, S. R., Schiavon, R. P., Frinchaboy, P. M., et al. 2017, AJ, 154, 94
Mapelli, M., Vallenari, A., Jeffries, R. D., et al. 2015, A&A, 578, A35
Marigo, P., Girardi, L., Bressan, A., et al. 2017, ApJ, 835, 77
Martig, M., Bournaud, F., Teyssier, R., et al. 2009, ApJ, 707, 250
Martig, M., Bournaud, F., Croton, D. J., et al. 2012, ApJ, 756, 26
Meléndez, J., & Barbuy, B. 2009, A&A, 497, 611
Mermilliod, J.-C., Andersen, J., Latham, D. W., et al. 2007, A&A, 473, 829
Mermilliod, J. C., Mayor, M., & Udry, S. 2008, A&A, 485, 303
Minchev, I., Chiappini, C., & Martig, M. 2013, A&A, 558, A9
Minchev, I., Chiappini, C., & Martig, M. 2014a, A&A, 572, A92
Minchev, I., Chiappini, C., Martig, M., et al. 2014b, ApJ, 781, L20
Ness, M., Hogg, D. W., Rix, H.-W., et al. 2016, ApJ, 823, 114
Netopil, M., Paunzen, E., Heiter, U., et al. 2016, A&A, 585, A150
Pastorelli, G., Marigo, P., Girardi, L., et al. 2020, MNRAS, 498, 3283
Reddy, A. B. S., Lambert, D. L., & Giridhar, S. 2016, MNRAS, 463, 4366
Reid, M. J., Menten, K. M., Brunthaler, A., et al. 2014, ApJ, 783, 130
Ruffoni, M. P., Den Hartog, E. A., Lawler, J. E., et al. 2014, MNRAS, 441, 3127
Schlafly, E. F., & Finkbeiner, D. P. 2011, ApJ, 737, 103
Sim, G., Lee, S. H., Ann, H. B., et al. 2019, J. Korean Astron. Soc., 52, 145
Smiljanic, R., Romano, D., Bragaglia, A., et al. 2016, A&A, 589, A115
Spina, L., Randich, S., Magrini, L., et al. 2017, A&A, 601, A70
Spina, L., Nordlander, T., Casey, A. R., et al. 2020, ApJ, 895, 52
Spina, L., Ting, Y.-S., De Silva, G. M., et al. 2021, MNRAS, 503, 3279
Soubiran, C., Bienaymé, O., & Siebert, A. 2003, A&A, 398, 141
Soubiran, C., Cantat-Gaudin, T., Romero-Gómez, M., et al. 2018, A&A, 619, A155
Sousa, S. G., Santos, N. C., Adibekyan, V., et al. 2015, A&A, 577, A67
Sun, Q., Deliyannis, C. P., Steinhauer, A., et al. 2020, AJ, 159, 220
Taylor, M. B. 2005, in Astronomical Data Analysis Software and Systems XIV, 347, 29
Torres, G., Andersen, J., & Giménez, A. 2010, A&ARv., 18, 67
Yana Galarza, J., Meléndez, J., Lorenzo-Oliveira, D., et al. 2019, MNRAS, 490, L86
Zhang, J., Zhao, J., Oswalt, T. D., et al. 2019, ApJ, 887, 84

Appendix A: Data and results on individual stars

Table A.1. Information on the observed targets based on Gaia DR2.

Name	Gaia ID	Ra (J2000)	Dec (J2000)	Gmag	BP-RP	Obs date	MJD-Obs	exp time (s)
ASCC 11	241730418805573760	03:32:04.87	+44:57:45.4	8.3675	1.507	2018-12-16	58468.84	1200
						2018-12-16	58468.82	1200
Alessi 1_1	402506369136008832	00:53:15.44	+49:31:53.8	9.824	1.187	2018-12-19	58471.82	1800
						2018-12-19	58471.84	1800
Alessi 1_2	402505991178890752	00:53:20.38	+49:28:49.7	9.808	1.176	2018-12-19	58471.87	1800
						2018-12-19	58471.89	1800
Alessi 1_3	402867593065772288	00:54:51.06	+49:53:17.2	9.565	1.186	2018-12-18	58470.86	1500
						2018-12-18	58470.88	1500
Alessi 1_4	402880684126058880	00:54:10.20	+49:40:08.9	7.099	1.349	2018-12-19	58471.93	1800
						2018-12-19	58471.95	1800
Alessi-Teusch 11	2184332753719499904	20:16:22.4	+52:06:18.4	7.099	1.349	2019-08-15	58710.86	690
Basel 11b_1	3424056131485038592	05:58:08.10	+21:57:44.7	10.989	1.782	2019-01-30	58513.90	3600
Basel 11b_2	3424055921028900736	05:58:10.12	+21:57:23.2	11.256	1.876	2019-01-30	58513.95	1800
						2019-01-30	58513.97	1800
						2019-01-30	58513.99	1800
Basel 11b_3	3424057540234289408	05:58:18.16	+21:58:43.7	11.320	1.884	2018-12-20	58472.19	1800
						2018-12-20	58472.21	1800
						2018-12-20	58472.24	1800
						2018-12-20	58472.26	1800
COIN-Gaia 30	532533682228608384	01:24:05.26	+70:25:25.1	8.352	1.762	2019-12-07	58824.85	1400
Collinder 463_1	534207555539397888	01:33:49.45	+71:51:09.6	7.946	1.632	2018-12-19	58471.80	1200
Collinder 463_2	534363067715447680	01:45:09.15	+71:53:25.3	7.725	1.572	2018-12-17	58469.81	1200
Gulliver 18	1836389309820904064	20:11:43.9	26:35:07.0	8.964	2.178	2019-08-10	58705.88	1380
Gulliver 24	430035249779499264	00:04:28.47	+62:42:04.4	10.494	1.927	2019-08-12	58707.15	1500
						2019-08-12	58707.16	1500
Gulliver 37	2024469226291472000	19:28:18.44	+25:22:53.4	10.592	1.559	2019-08-13	58708.94	608
						2019-08-13	58708.93	1500
NGC 2437_1	3029609393042459392	07:41:36.9	-14:26:11.2	10.277	1.338	2018-12-17	58469.08	1800
						2018-12-17	58469.10	1800
NGC 2437_2	3029202711180744832	07:41:28.52	-14:54:17.5	10.293	1.285	2018-12-17	58469.12	1800
						2018-12-17	58469.15	1800
NGC 2437_3	3030364134752459904	07:41:00.64	-14:12:08.4	10.417	1.274	2018-12-17	58469.17	1800
						2018-12-17	58469.19	1800
NGC 2437_4	3029132686034894592	07:42:47.85	-15:17:44.16	10.838	1.302	2018-12-18	58470.18	2400
						2018-12-18	58470.20	2400
NGC 2437_5	3029156222454419072	07:42:41.24	-14:59:51.4	10.948	1.262	2018-12-19	58471.17	2400
						2018-12-19	58471.20	2400
NGC 2437_6	3029207006148017664	07:41:19.42	-14:48:47.5	9.877	1.332	2018-12-18	58470.10	1500
						2018-12-18	58470.12	1500
NGC 2437_7	3029226694277998080	07:41:19.36	-14:40:59.7	9.975	1.322	2018-12-08	58470.14	1500
						2018-12-08	58470.16	1500
NGC 2509	5714209934411718784	08:00:44.36	-19:06:59.4	12.883	1.275	2019-01-15	58498.07	2400
						2019-01-15	58498.10	2400
						2019-01-15	58498.13	2400
NGC 2548_1	3064481400744808704	08:13:35.42	-05:53:02.04	9.377	1.098	2018-12-17	58469.24	1200
						2018-12-17	58469.25	1200
NGC 2548_2	3064537647636773760	08:12:37.24	-05:40:51.0	9.151	1.111	2018-12-18	58470.24	1200
						2018-12-18	58470.25	1200
NGC 2548_3	3064579703955646976	08:14:28.10	-05:42:16.09	9.187	1.190	2018-12-19	58471.23	1200
						2018-12-19	58471.25	1200
NGC 2548_4	3064486692144030336	08:13:40.44	-05:46:24.96	8.873	0.786	2018-12-17	58469.27	1800
NGC 7082_1	1972288740859811072	21:28:48.97	+47:06:54.2	8.171	1.508	2019-12-08	58825.80	1400
NGC 7082_2	1972288637780285312	21:28:34.58	+47:05:22.92	7.622	1.470	2019-12-07	58824.81	1400
NGC 7209_1	1975004019170020736	22:05:09.94	+46:31:25.3	9.766	1.323	2019-08-14	58709.14	1725
						2019-08-14	58709.16	1725

Table A.1. continued.

Name	Gaia ID	Ra (J2000)	Dec (J2000)	Gmag	BP-RP	Obs date	MJD-Obs	exp time (s)
NGC 7209_2	1975002919658397568	22:05:17.63	+46:29:00.6	8.891	1.734	2019-08-14	58709.12	2070
Tombaugh 5_1	473266779976916480	03:47:30.99	+59:02:50.8	11.163	2.123	2018-12-20	58472.11	1800
						2018-12-20	58472.09	1800
						2018-12-20	58472.15	1800
						2018-12-20	58472.13	1800
Tombaugh 5_2	473275782228263296	03:48:32.98	+59:15:16.56	11.366	2.147	2019-01-15	58497.06	1800
						2019-01-14	58497.04	1800
						2019-01-15	58498.00	1800
Tombaugh 5_3	473268424940932864	03:47:46.78	+59:05:36.6	11.138	2.028	2019-01-14	58498.03	1800
						2019-01-14	58497.98	1800
						2019-01-14	58497.02	1800
UPK 219	2209440823287736064	23:30:29.72	+65:08:35.3	8.728	1.734	2019-12-08	58825.84	1400
			Comparison clusters					
Collinder 350_1	4372743213795720704	17:46:24.88	+01:02:39.7	5.957	1.869	2018-08-20	58350.87	300
						2018-08-20	58350.88	300
Collinder 350_2	4372572888274176768	17:48:43.82	+01:09:51.1	8.421	1.485	2018-08-20	58350.88	1380
NGC 2682_1	604921512005266048	08:51:26.17	+11:53:51.9	10.202	1.238	2020-02-02	58881.07	1500
						2020-02-02	58881.08	1500
NGC 2682_2	604920202039656064	08:51:59.51	+11:55:04.8	10.205	1.243	2020-02-02	58881.10	1500
						2020-02-02	58881.12	1500
NGC 2682_3	604904950611554432	08:51:50.19	+11:46:06.9	10.511	1.110	2020-02-02	58881.14	1500
						2020-02-02	58881.16	1500
						2019-12-08	58825.19	1500
						2019-12-08	58825.21	1500
						2019-12-08	58825.22	1500
						2020-03-11	58919.04	1500
						2020-03-11	58919.06	1500
NGC 2682_4	604917728138508160	08:51:23.76	+11:49:49.3	11.231	1.073	2020-03-10	58918.99	1420
						2020-03-11	58919.00	1420
						2020-03-11	58919.02	1420

Table A.2. Final atmospheric parameters of observed targets

Name	Gaia ID	$T_{\rm eff}$ (K)	$\sigma\ T_{\rm eff}$	log g (dex)	σ log g	[Fe/H] (dex)	σ_1 [Fe/H]	σ_2 [Fe/H]	log ϵ Fe I	std	Nlines Fe I	log ϵ Fe II	std	Nlines Fe II	v_{micro} (km s^{-1})	σ v_{micro}
ASCC 11	241730418805573760	5250	70	2.15	0.10	−0.14	0.05	0.06	7.360	0.159	46	7.360	0.210	10	2.4	0.3
Alessi 1_1	402506369136008832	5000	70	2.65	0.15	−0.10	0.05	0.05	7.392	0.181	74	7.391	0.136	16	1.5	0.1
Alessi 1_2	402505991178890752	5200	70	3.20	0.10	0.08	0.10	0.10	7.583	0.135	75	7.587	0.128	15	1.5	0.2
Alessi 1_3	402867593065772288	5250	65	3.27	0.10	0.07	0.06	0.06	7.576	0.105	75	7.575	0.098	15	1.6	0.1
Alessi 1_4	402880684126058880	5120	60	3.09	0.06	−0.05	0.10	0.10	7.470	0.122	72	7.476	0.089	16	1.6	0.1
Alessi-Teusch 11	2184332753719499904	4560	50	2.10	0.15	−0.19	0.05	0.05	7.310	0.172	75	7.311	0.219	16	2.1	0.2
Basel 11b_1	3424056131485038592	5180	50	3.15	0.13	0.00	0.05	0.05	7.500	0.093	68	7.507	0.127	13	2.2	0.1
Basel 11b_2	3424055921028900736	5220	30	3.07	0.10	0.02	0.03	0.03	7.525	0.141	72	7.529	0.135	15	2.2	0.2
Basel 11b_3	3424057540234289408	4950	50	2.83	0.10	−0.04	0.05	0.05	7.464	0.136	77	7.467	0.116	15	2.1	0.1
COIN-Gaia 30	532533682228608384	5200	50	3.40	0.05	0.03	0.05	0.05	7.538	0.158	71	7.552	0.163	15	2.3	0.2
Collinder 463_1	534207555539397888	4730	30	2.12	0.10	−0.20	0.05	0.05	7.310	0.130	72	7.310	0.180	16	2.5	0.1
Collinder 463_2	534363067715447680	4730	30	2.30	0.15	−0.10	0.05	0.05	7.410	0.131	70	7.410	0.207	16	2.4	0.1
Gulliver 18	1836389309820904064	4590	100	2.60	0.17	−0.10	0.04	0.05	7.409	0.212	76	7.395	0.281	16	2.8	0.3
Gulliver 24	430035249779499264	4450	50	2.50	0.15	−0.18	0.03	0.03	7.317	0.145	74	7.316	0.240	16	2.0	0.2
Gulliver 37	2024469226291472000	4850	50	3.65	0.12	0.10	0.03	0.04	7.602	0.213	62	7.604	0.403	10	0.8	0.6
NGC 2437_1	3029609393042459392	5050	50	2.77	0.12	0.04	0.05	0.05	7.546	0.142	64	7.548	0.109	12	2.1	0.1
NGC 2437_2	3029202711180744832	5250	75	3.32	0.10	0.07	0.05	0.05	7.572	0.140	62	7.578	0.171	13	2.2	0.2
NGC 2437_3	3030364134752459904	5300	110	3.13	0.10	−0.05	0.05	0.05	7.450	0.176	62	7.447	0.149	13	2.3	0.2
NGC 2437_4	3029132686034894592	5085	65	2.90	0.10	0.00	0.05	0.05	7.508	0.111	62	7.498	0.089	15	1.7	0.1
NGC 2437_5	3029156222454419072	5030	75	2.85	0.15	0.00	0.10	0.10	7.503	0.163	74	7.505	0.161	16	1.7	0.1
NGC 2437_6	3029207006148017664	4990	65	2.72	0.10	0.00	0.05	0.06	7.443	0.238	72	7.444	0.266	15	2.1	0.1
NGC 2437_7	3029226694277998080	4650	90	2.27	0.20	−0.07	0.08	0.08	7.440	0.216	73	7.440	0.272	16	1.2	0.1
NGC 2509	5714209934411718784	4705	40	2.53	0.20	−0.10	0.05	0.06	7.394	0.213	72	7.392	0.330	16	1.5	0.3
NGC 2548_1	3064481400744808704	5370	70	3.67	0.15	0.00	0.05	0.05	7.507	0.131	60	7.504	0.155	15	2.0	0.2
NGC 2548_2	3064537647636773760	5050	50	2.65	0.10	−0.02	0.04	0.04	7.479	0.068	62	7.480	0.101	15	1.6	0.1
NGC 2548_3	3064579703955646976	4930	50	2.70	0.10	−0.01	0.05	0.05	7.490	0.079	61	7.491	0.083	13	1.6	0.1
NGC 2548_4	3064486692144030336	5200	50	3.18	0.10	−0.07	0.07	0.07	7.434	0.110	62	7.439	0.142	14	0.4	0.1
NGC 7082	1972288740859811072	4994	50	2.25	0.1	−0.15	0.05	0.07	7.360	0.144	63	7.361	0.199	12	3.0	0.2
NGC 7209_1	1975004019170020736	4880	50	2.35	0.15	0.00	0.03	0.07	7.439	0.110	74	7.433	0.155	16	1.7	0.2
NGC 7209_2	1975002919658397568	4600	30	2.79	0.15	−0.07	0.05	0.05	7.433	0.136	67	7.435	0.316	16	2.5	0.2
Tombaugh 5_1	473266779976916480	5010	50	3.17	0.15	0.04	0.05	0.05	7.543	0.166	72	7.546	0.185	15	2.2	0.1
Tombaugh 5_2	473275782228263296	4900	50	2.31	0.1	−0.07	0.05	0.01	7.438	0.080	74	7.436	0.073	14	2.0	0.2
Tombaugh 5_3	473266779976916480	5150	50	3.08	0.15	0.07	0.05	0.05	7.570	0.095	69	7.576	0.147	15	2.2	0.2
UPK 219	2209440823287736064	5203	150	3.01	0.10	0.02	0.05	0.05	7.528	0.166	74	7.530	0.283	16	2.7	0.2
Collinder 350_1	4372743213795720704	4200	50	1.30	0.20	−0.40	0.08	0.08	7.120	0.149	71	7.130	0.256	16	2.2	0.1
Collinder 350_2	4372572888274176768	5300	50	3.15	0.1	0.02	0.05	0.05	7.521	0.079	71	7.526	0.095	15	1.6	0.1
NGC 2682_1	604921512005266048	4687	50	2.37	0.07	−0.05	0.05	0.05	7.454	0.174	75	7.453	0.181	16	1.5	0.2
NGC 2682_2	604920202039656064	4900	110	2.76	0.1	0.02	0.05	0.05	7.520	0.132	69	7.528	0.168	15	1.7	0.2
NGC 2682_3	604904950611554432	5000	50	2.77	0.1	−0.03	0.03	0.03	7.467	0.096	67	7.467	0.082	14	1.2	0.2
NGC 2682_4	604917728138508160	5195	50	3.25	0.10	0.00	0.05	0.03	7.501	0.108	67	7.502	0.164	14	1.3	0.2
SUN		5770	40	4.44	0.08	−0.03	0.03	0.03	7.477	0.077	76	7.477	0.083	16	1.0	0.1

Notes. $\sigma_1[Fe/H]$ is the error from metallicity measurement, $\sigma_2[Fe/H]$ is the deviation of iron abundance combined to the uncertainties of EW and error in metallicity determination.